NANO FUTURES

TOPICAL REVIEW

Carbon nanotube electronics for IoT sensors

RECEIVED
21 August 2019

ACCEPTED FOR PUBLICATION
5 December 2019

PUBLISHED
10 January 2020

Jorge A Cardenas[1], Joseph B Andrews[1], Steven G Noyce[1] and Aaron D Franklin[1,2]

[1] Department of Electrical and Computer Engineering, Duke University, Durham NC 27708, United States of America
[2] Department of Chemistry, Duke University, Durham NC 27708, United States of America

E-mail: aaron.franklin@duke.edu

Keywords: carbon nanotubes, Internet of Things, sensors, transistors, flexible electronics, printed electronics

Abstract

The Internet of Things (IoT) is the concept of a ubiquitous computing ecosystem in which electronics of custom form factors are seamlessly embedded into everyday objects. At the heart of the IoT are electronic sensors capable of detecting physical/environmental phenomena, translating these measurements into electrical signals, and wirelessly transmitting the data for remote computing. Critical to the development of IoT sensors and systems are low-cost materials, robust enough to sustain stable electrical performance over medium to long periods of time, yet sensitive enough to detect small changes in the surrounding environment. Such materials should be mechanically flexible and amenable to solution-based processing to facilitate large scale production methods, such as roll-to-roll printing. Carbon nanotubes (CNTs) are one of the leading material candidates to satisfy these requirements because of their unique electrical and mechanical properties, which enable robust and versatile devices, in combination with their chemical properties, which allow for the processing of CNTs from solution. These advantages have enabled demonstration of a myriad of printed CNT-based electronics and sensors on diverse substrates with wide ranges of functionality, spanning from simple sensors based on passive devices to complex multi-stage circuitry and display electronics. In this review, we provide a comprehensive summary of the CNT-based electronics and sensor space with an emphasis on applications aligned with the IoT. Primary coverage is devoted to devices consisting of randomly oriented CNT networks; however, the advantages and capabilities of single-nanotube devices will also be discussed. Key works across various types of sensors will be reviewed and a summary of the remaining challenges for CNT-based sensor technologies will be presented.

1. Introduction

The phrase 'Internet of Things' (IoT) was first coined in 1999 by Kevin Ashton in a presentation linking the then-new idea of radio frequency identification (RFID) to supply chain management [1]. Today, the IoT concept has broadly expanded to include a wide range of applications across various fields, including healthcare, utilities, manufacturing, and transportation [2]. The concept of the IoT describes the computing paradigm wherein sensors and actuators are seamlessly embedded into everyday objects (or 'things'), and the data collected from these embedded sensors is wirelessly shared across platforms to create a common picture of the environment. The data collected from this ubiquitous sensor network can then be stored or processed remotely, from which autonomous decisions can be made to create an embedded intelligence within the environment [3]. Whereas the first Internet revolution led to the interconnection between people, the IoT will lead to the interconnection between objects.

Critical to the growth of the IoT is the development of the hardware necessary to sense, process, and transmit data in a low-power, low-cost manner [4]. Such hardware can come in the form of RFID technologies or wireless sensor networks. However, the sensor hardware lies at the lowest level of the network and will form the nervous system of the IoT infrastructure. As such, it is imperative that each sensor system is robust enough to sustain stable electrical performance over medium to long periods of time, yet sensitive enough to detect small changes in the environment, all while being seamlessly embedded into a host object in a thin and mechanically flexible

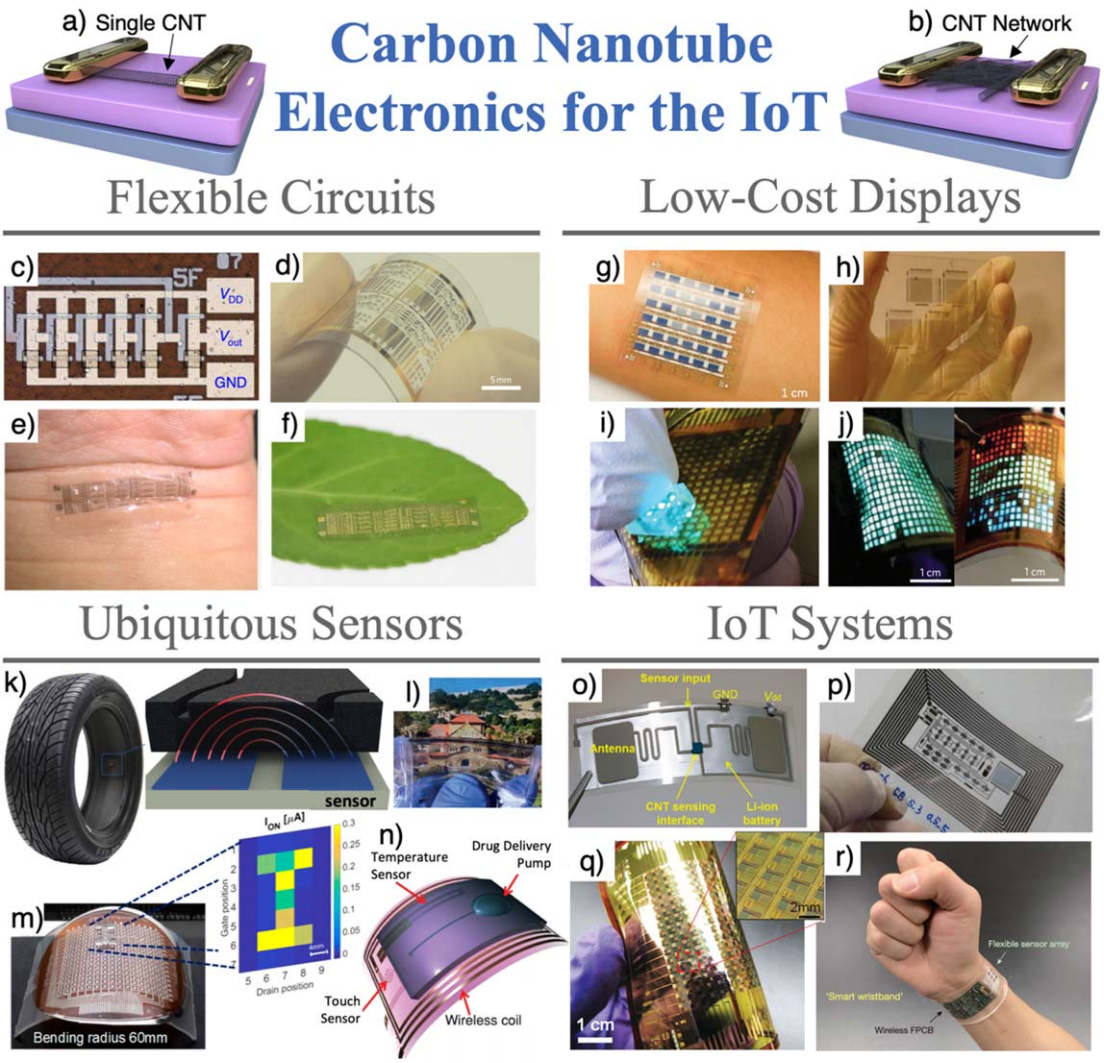

Figure 1. Overview of carbon nanotube-based devices in the IoT space. Major CNT applications include flexible circuits (ring oscillators, digital logic, etc), low-cost displays (active matrix backplanes), ubiquitous sensors (physical, chemical, biological), and IoT systems (antennas, wearables, etc). (a), (b) Reproduced and adapted from [13]. (c) Reproduced and adapted from [24]. (d) Reproduced and adapted from [16]. (e), (f) Reproduced and adapted from [25]. (g) Reproduced and adapted from [26]. (h) Reproduced and adapted from [27]. (i), (j) Reproduced and adapted from [15]. (k) Reproduced and adapted from [21]. (l) Reproduced and adapted from [19]. (m) Reproduced and adapted from [28]. (n) Reproduced and adapted from [22]. (o) Reproduced and adapted from [29]. (p) reproduced and adapted from [30]. (q) Reproduced and adapted from [9]. (r) Reproduced and adapted from [23].

manner, without disrupting form factor or appearance. A large variety of demonstrations of flexible sensors have already been developed for IoT applications, including pressure/strain sensors [5], temperature sensors [6], and chemical/gas sensors [7]. A primary challenge that remains in creating sensor networks that can facilitate an IoT ecosystem is developing a sensor technology that is mass-manufacturable, able to capture the desired data with sufficient accuracy, and low-cost enough to become ubiquitous [8].

One of the most prevalent electronic materials that can potentially satisfy each of the abovementioned requirements to enable an IoT sensor technology are carbon nanotubes (CNTs) [9]. CNTs are 1D allotropes of carbon that possess extraordinary electrical, mechanical, and chemical properties, such as extremely high carrier mobility [10], flexibility [11], chemical stability [12, 13], as well as compatibility with solution phase processing [14]. The electrical and mechanical properties of CNTs have been exploited in the development of a myriad of flexible electronics demonstrations, including the operation of large-scale circuitry and displays [15–17]. Meanwhile, the chemical properties of carbon nanotubes have been exploited in the development of stable and functional inks for printed electronics [18]. Through printing, CNT-based technologies have the potential to be low-cost and mass-manufacturable. Due to these distinct advantages, along with the inherently high sensitivity of carbon nanotubes owed to their nanoscale nature, a large amount of research has been invested into the development of CNT-based sensors. These include demonstrations of flexible strain sensors for electronic skins [19], capacitive sensors for tire tread thickness monitoring [20, 21], and low-cost biosensors for point-of-care diagnostics [22, 23], just to name a few. Several of these demonstrations are highlighted in figure 1, which

outlines many of the ways in which CNT-based electronics, sensors, and displays have been utilized in producing IoT systems.

In this review, we provide a comprehensive summary of the CNT-based electronics and sensor space with an emphasis on applications aligned with the IoT. This work is divided into four sections, the first of which will outline CNT properties, synthesis, and deposition methods, including printing. The second section will outline CNT-based electronics, ranging from simple passive devices to complex, multi-stage circuitry and display electronics. The third section will outline the CNT-sensor space, drawing on key works from the literature in presenting the most IoT-relevant sensor demonstrations. Finally, the fourth section will highlight remaining challenges and the outlook moving forward with CNT-based electronics in the IoT, including device variability, stability, and competing materials. Primary coverage of CNT-based electronics is devoted to devices that rely on randomly oriented CNT networks, often used in thin-film transistors (TFTs). However, aligned single or few nanotube-based nanoscale devices will also be discussed, which find primary use in nanoscale field-effect transistors (herein referred to as CNT-FETs).

2. Carbon nanotubes

2.1. Properties

With regards to their bond structure, CNTs are very similar to graphene, in that both share sp^2 bond hybridization; however, the differences in CNTs stem from their 1D geometry. A CNT can be considered as a sheet of graphene 'rolled up' into a seamless 1D cylinder. The diameter and electronic properties of a nanotube are dependent upon its chiral vector, which is a circumferential vector associated with the angle in which the CNT is 'rolled up.' The chiral vector can be described as $\mathbf{c} = n\mathbf{a} + m\mathbf{b}$, where **a** and **b** are two unit vectors that define the location of all atoms in a honeycomb lattice [31]. The set of possible chiral vectors for CNTs are depicted figure 2(a), which also highlights the dependence of a CNTs electronic properties on the chiral vector. CNTs can exist in a variety of structural configurations, including armchair (n, n), zig-zag (n, 0), and chiral (n, m), each of which is illustrated in figure 2(b).

The electronic behavior of a CNT is determined by the projection of its 1D subbands (the orientation of which is determined by the chiral vector) onto graphene's 2D energy dispersion space. As can be seen in figure 2(a), for every chiral vector resulting in metallic behavior, there are two chiral vectors that result in semiconducting behavior. Statistically, in an uncontrolled synthesis process, the electronic yield of metallic to semiconducting CNTs is 1:2. There are many methods to synthesize carbon nanotubes, the most prominent of which are arc discharge [36], laser ablation [37], plasma torch [38], and chemical vapor deposition (CVD) [39]. CVD is one of the most commonly used methods for CNT synthesis and will be the only method discussed in this work. The presence of metallic tubes after CNT synthesis presents a fundamental challenge, since it is the semiconducting properties of CNTs that are most often desired for electronics applications. The following sections describe the methods in which CNTs are synthesized and sorted based upon chirality or electronic type.

2.2. Synthesis and orientation

Many applications benefit from the synthesis of single-walled CNTs (SWCNTs or simply CNTs herein) that are already aligned on a substrate, ready for fabrication of devices with either one or any number of parallel nanotubes [40]. In comparison to devices based on CNT network thin films, these devices from aligned nanotubes avoid added resistance and other effects that arise from the CNT to CNT junctions and longer percolation conduction paths [41]. The methods most commonly used to synthesize CNTs aligned on a substrate involve catalytic CVD. The most prevalent of these consists of annealing ST-cut quartz to promote the formation of step edges, depositing patterned lines of iron catalyst nanoparticles, and synthesizing CNTs by CVD in a tube furnace with the gas flow running parallel to the quartz nano-steps [42]. The steps in the quartz substrate guide the growing CNTs along straight lines, aligned in a consistent direction. The resulting CNTs are aligned, but the spacing between CNTs is not consistent. This process has been frequently carried out up to the wafer scale [43]. Once synthesized, these aligned CNTs can either be used as-grown on the quartz substrate, or more frequently transferred onto a separate device substrate [44–46].

With proper catalyst control, it may be possible for a CVD process to be designed that synthesizes aligned CNTs of one uniform chirality; however, current techniques result in aligned CNTs with a distribution of diameters [47]. Hence, at the very least the metallic CNTs must be removed before semiconducting devices can be created. Several sorting methods have been developed specifically for use in the case of aligned CNTs on a substrate. The simplest of these is referred to as 'burn-out', where devices are fabricated containing a mixture of metallic and semiconducting CNTs, after which the gate is used to limit the conductance of semiconducting CNTs while large currents are flowed through the metallic CNTs, leading to joule heating and oxidative destruction of the metallic CNTs [48, 49]. A more refined version of this process relies on a lower current causing

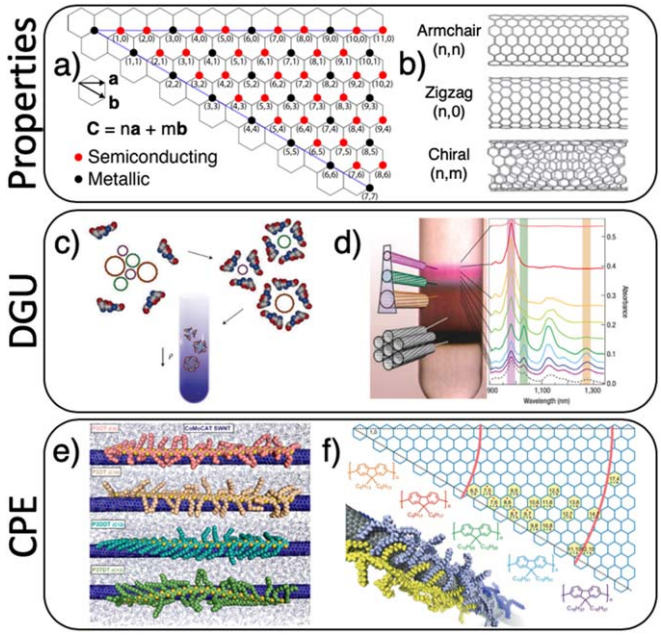

Figure 2. Structural properties between various carbon nanotubes and their sorting methods. (a) Set of possible chiral vectors for CNTs with red dots indicating semiconducting behavior and black dots indicating metallic behavior. (b) Schematic of the various structures that CNTs can have, depending on the chiral vector. Reproduced from [32] (c) Schematic illustrating how increasing amounts of small molecules attach to CNTs of increasing diameter in DGU. (d) Schematic showing how various regions of a DGU-sorted solution exhibit different absorption spectra. (c), (d) Reproduced and adapted from [33]. (e) Illustration of the conjugated polymer wrapping of CNTs. Reproduced and adapted from [34]. (f) Schematic showing how various conjugated polymers can select for CNTs of specific properties. Reproduced and adapted from [35].

a small amount of joule heating that causes thermocapillary flows in a resist layer, uncovering the metallic CNTs and allowing them to be selectively etched by another process, such as oxygen plasma [50]. A third method causes joule heating in metallic CNTs by exposing the growth wafer to microwave radiation after metal antennas have been fabricated [51]. The main advantage of this last approach is that complete devices need not be fabricated prior to the sorting step. These methods have been used by many groups to create high performance, nanoscale devices [52–54].

For producing SWCNTs at larger scale, other catalytic CVD-based synthesis variations have been developed for growing CNTs without strict alignment on a substrate. Such methods include production technologies such as HiPCO and CoMoCAT, which involve the use of an energy source, transition metal catalyst particles, and a carbon feedstock in the gas-phase [55]. Many of these methods have some degree of control over the CNT properties, as the diameters of the nanotubes are related to the size of the metallic nanoparticles used in the synthesis process. Once the CNTs have been synthesized, a variety of purification steps, such as acid treatment and filtration, are required to remove excess impurities and catalyst particles in order to form a usable product, often in the form of a powder.

2.3. Solution-phase sorting

Although there has been significant progress in the controlled growth of CNTs with specific electronic properties, the purity and yield of controlled growth processes have not sufficiently satisfied the requirements of most electronic applications, especially those at large scale [41]. Alternatively, the primary means of producing large quantities of CNTs with sufficient purity for thin-film and printing applications has been to use post-synthesis solution-phase sorting methods, which can sort solutions of CNTs at liter-scale throughputs [56]. There exists a large variety of CNT sorting methods, most of which were developed during the early 2000s, including density gradient ultracentrifugation (DGU) [33], gel electrophoresis [57], conjugated polymer extraction (CPE) [58], ion-exchange chromatography [59], and aqueous two-phase extraction [60], among others, which can select for specific nanotube chiralities, lengths, diameter and even handedness [32, 61]. The two methods that will be covered in this work are DGU, for its historical significance as it was the first solution-phase sorting method to be developed, and CPE, for its current relevance and use in large scale production.

DGU was first demonstrated by Arnold *et al* [33], where heterogenous CNT mixtures in solution were discriminated by structure using ultracentrifugation. Bile salts or surfactants (often sodium cholate or sodium dodecyl sulfate) can be introduced into CNT solutions and encapsulate CNT species to varying degrees, depending on the structure and diameter of the tubes. This process is illustrated in figure 2(c), where it can be

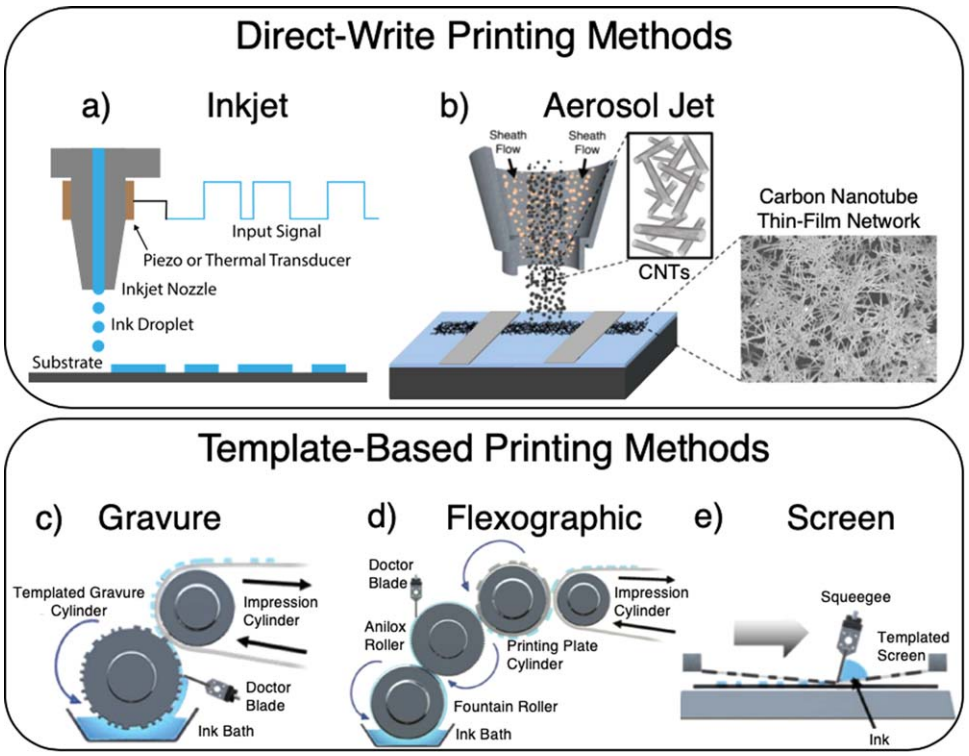

Figure 3. Methods for printing CNTs across both direct-write and template-based processes. (a) Schematic diagram and operation of an inkjet print head. (b) Schematic diagram of an aerosol jet printhead including device schematic with SEM image of CNT thin film. (b) Reproduced and adapted from [69]. Schematic diagrams of the (c) gravure, (d) flexographic, and (e) screen printing processes. (c)–(e) Reproduced and adapted from [70].

seen that a larger number of salt/surfactant molecules will wrap around CNTs of larger diameters, creating differences in buoyant densities across CNTs with varying structures. Applying ultracentrifugation to the CNT/surfactant solution can then create a spatial density gradient across the solution, where various regions of the medium have a homogenous distribution of CNT diameters. An image of a density gradient medium is shown in figure 2(d), where it can be seen that different regions of the medium exhibit distinct absorbance spectra, corresponding to the differences in CNT properties in each region. A variety of other DGU-based strategies can also be used to discriminate CNTs of various lengths [62] and handedness [63]. However, compared to other sorting methods, DGU is relatively inefficient and costly, as it typically requires multiple iterations to achieve solutions of sufficiently high purity [64].

In contrast to DGU, CPE sorts CNTs using conjugated polymers often derived from polyfluorene (PFO) [35, 58] or poly(3-alkylthiophene)s (P3AT) [34], which are highly selective for specific CNT properties. The π-conjugated backbone of polymer molecules can selectively interact with the graphene-like π-bond surface of nanotubes with specific electronic properties while the polymer side chains encapsulates the CNTs and supports dispersion in organic solvents (an illustration can be seen in figure 2(e)). The CPE process has some degree of chiral selectivity, as shown in figure 2(f), depending upon the chemical structure of the conjugated polymer. The CPE process is often quite simple, only consisting of sonication of a CNT/polymer solution, centrifugation in order to sediment unwanted species, and collection of the desired s-CNT supernatant [65]. Due to its simplicity, CPE is often combined with other sorting processes, such as silica gel adsorption, as demonstrated by Ding *et al* [66], to enhance purity. Due to the simplicity, high selectivity, and high yield, CPE and its hybrids are particularly interesting for large-scale electronic applications; however, challenges remain associated with understanding the mechanism of sorting using conjugated polymers, which will be necessary to eventually sort CNTs of specific chiral angles and uniform bandgaps which could be generally useful for numerous device applications not limited to sensors [65, 67].

2.4. Solution-phase deposition and printing

With the development of sorted CNTs from solution, there remains the challenge of depositing and assembling CNTs from solution phase. As can be expected, when CNT solutions are deposited on a substrate and the carrier solvent evaporates, what remains is a network of randomly oriented tubes. For device applications that rely only on a single CNT, the concentration of the CNT solution must be sparse enough so that when the CNTs

precipitate out of solution, there remains a low density dispersion of CNTs from which devices can be constructed. However, for thin-film applications, the randomly oriented CNTs must form a film with sufficient density so that nanotubes overlap and electronic percolation can occur. An SEM image of a randomly oriented thin film of CNTs can be seen in the inset of figure 3(b). Although individual nanotubes can exhibit ballistic transport and possess mobilities exceeding 100 000 $cm^2 V^{-1} s^{-1}$ [10], electronic transport through a CNT thin film is limited by the tube-to-tube junctions present throughout the network [68]. Additionally, there often exists an organic residue present throughout a solution-deposited film from the remnant of the polymer used to stabilize the CNTs in solution. Typically, an additional rinse with solvent is necessary after film deposition in order to remove these excess organics. Common CNT network mobilities lie between 1 and 100 $cm^2 V^{-1} s^{-1}$, depending on the tube density. Additional analysis of this topic is given in later sections of this report.

Prior to the deposition of CNT films, most substrates require some surface preparation, such as cleaning using an O_2 plasma or functionalization with poly-L-lysine (PLL) [71] or aminopropyltriethoxy silane (APTES) [72] for CNT adhesion. The most classic of the solution-phase deposition methods are substrate incubation, drop-casting, or spin-coating. Recent demonstrations of the incubation method have been shown to produce highly uniform films of CNTs with high tunability of the film density depending on the incubation time [73]. The drawback associated with substrate incubation, as well as all other classical CNT film deposition methods, is the inability to selectively pattern the deposited film. In most cases, unwanted regions of CNTs must be removed using an O_2 plasma. Methods such as spin coating have been used to deposit CNT films with some degree of alignment, but also suffer from little to no control over film pattern. While simple methods, such as drop-casting, have some degree of control over the pattern of the deposited film, typically these films suffer from poor uniformity.

Over the past 20 years, a number of printing techniques have been developed for directly depositing electronic inks from solution, including CNT inks. There exist many different methods of printing, all of which can be divided between two categories: direct-write printers and template-based printers, schematic illustrations of which are in figure 3. Direct-write printers are well suited for low-to-medium throughput production environments, where rapid customization and agility are required. Direct-write printers do not rely on the use of a mask or template and can selectively deposit ink through a fine-tipped nozzle to generate patterns using computer-controlled motion. The class of direct-write printers includes inkjet, aerosol jet, syringe, and electrohydrodynamic printers, among others, all which are capable of writing features at the 10–1000 μm scale. Among these printers, CNT inks are most commonly printed using inkjet and aerosol jet methods.

Deposition through an inkjet printhead nozzle (illustrated in figure 3(a)) relies on a thermoelectric or piezoelectric transducer, which propels a droplet out from the nozzle. With regards to printing CNTs and inks of other high-aspect ratio nanostructures, inkjet printers suffer from a propensity for nozzle clogging [74], which can limit throughput. Alternatively, aerosol jet printers (AJPs) have been shown to print CNT inks with high reproducibility and for long periods of time [75]. The advantages in printing high-aspect ratio nanostructures using AJPs can be attributed to their unique nozzle structure and operation, which is illustrated in figure 3(b). Once an ink aerosol is generated using ultrasonic or pneumatic atomization, this aerosol stream is directed down through the middle of the nozzle where it is met by a secondary inert sheath gas flow, which focuses the carrier gas stream as it is jetted out from the nozzle and prevents it from coming into contact with the nozzle sidewalls. Because of this sheath flow protection, AJPs have also been used to print other high-aspect ratio inks, such as low-temperature-compatible silver nanowires (AgNWs), without a propensity for nozzle clogging [76]. Furthermore, the merits of AJPs with respect to printing high-aspect ratio nanostructures, both AgNWs and CNTs, could enable fully low-temperature printed CNT-TFTs and the development of print-in-place electronics, where the substrate is never removed from the printer for external processing throughout the fabrication process [77].

Whereas direct-write printing methods are well suited for rapid prototyping and fabrication on nonplanar surfaces, template-based printers are better suited for medium- to high-throughput production environments as they rely on the use of masks or physical templates to stamp or transfer patterns of ink onto a substrate [70]. In many cases, these printers are compatible with roll-to-roll production processes where printing throughputs as high as tens of meters per second can be realized. The size scale of these printers can range from fitting onto desktops to taking up the space of an entire room, and the start-up costs and/or turn-around time associated with creating a physical mask or template can be quite high depending on its size and resolution. Template-based printers include gravure, flexographic, and screen printers, schematics of which are illustrated in figures 3(c)–(e). The inks that are compatible with this class of printers require strict rheological constraints in comparison to direct-write printers, such as high ink viscosity which necessitates the use of organic fillers which can limit electrical performance and require added thermal processing.

With respect to template-printing CNT-based inks, there have been relatively few demonstrations of semiconducting CNT inks and most work has been to devoted to conductive multi-walled carbon nanotube inks for electrochemical sensors [78]. The limitation associated with developing a semiconducting CNT ink are the

polymer binders that need to be incorporated into the ink to increase its viscosity. Adding these binders severely reduces thin-film performance; recent demonstrations have shown that films printed from such inks possess mobilities less than 1 $cm^2 V^{-1} s^{-1}$ [79]. To avoid this low-performance limitation in the printing of CNT-based devices from template-based methods, typically a blanket layer of CNTs is deposited using the incubation method, followed by the template-printing of the remaining dielectric and conductive layers [80]. It should also be noted that hybrid direct-write/template-based printing processes have been developed for fabricating CNT-TFTs, where the CNT layer is directly printed using an inkjet printer and the other layers are gravure printed [81].

3. Carbon nanotube electronics

3.1. Resistive/capacitive/electrochemical devices

The simplest forms of devices consisting of carbon nanotubes are two-terminal passive elements. These devices include resistors, capacitors, inductors, and diodes. With regards to sensing applications, restive and capacitive-based devices are most relevant. Carbon nanotube resistors can be powerful sensing elements due a nanotube's sensitivity to small changes in its surroundings. In the case of nanotube networks, film resistance is highly dependent upon the density of junctions throughout the film, which is changed (and can be monitored) with the application of strain. Capacitive elements, on the other hand, make use of carbon nanotubes as the electrode materials, where the nanomorphology of CNTs can be exploited to enhance sensitivity. Both resistive- and capacitive-based sensors will be discussed in ensuing sections herein. Also relevant to sensors are CNT-based electrochemical devices, which can exploit the nanotube's chemical and mechanical properties for chemical, gas, or biosensors. For these applications, the mechanical flexibility and excellent electro-catalytic behavior of the CNTs make them ideal for integration into flexible or wearable point-of-care sensors [78].

3.2. Nanoscale transistors (high performance)

While many IoT applications prioritize cost above performance, some applications require high-performance transistors, which can necessitate nanoscale fabrication approaches. Nanoscale CNT devices typically utilize aligned CNTs rather than films composed of random CNT networks. Scaling has long been a method of increasing transistor or chip-level performance, and complimentary CNT-FETs have been scaled down to 5 nm gate lengths [82, 83]. Feasibility of creating large-scale logic circuits has been demonstrated by creating a carbon nanotube computer [84]. Promise has also been shown for RF applications by demonstrating both a CNT radio [85] and a power amplifier with a current gain cut-off frequency above 100 GHz [86]. While CNT network devices are more frequently pointed to for their flexibility, devices composed of aligned CNTs have also shown high performance on flexible substrates [87].

While interest in CNTs for electronics was initially focused exclusively on nanoscale, high-performance transistors, there has been considerable evolution and broadening in the field. No longer are CNT-FETs seen wholly as a potential replacement for silicon in the push for smaller and better nanoscale transistors [48, 88]. Rather, even for high-performance applications, CNT-based transistors are seen as valuable for their combination of performance and versatile integration, such as being added to the back-end-of-line to create a 3D integrated circuit (IC) for boosting computational performance in a traditional microprocessor [89] or adding diverse functionality for a system-on-chip [90]. These integration approaches for CNT-based devices may well include other passive elements or TFTs from nanotubes, but the primary focus thus far has been on the high-performance CNT-FETs for these applications. Since there are needs in the growing IoT for lower power chips with higher computational performance, progress on custom integration approaches for high-performance CNT-FETs is worth watching.

3.3. Thin-film transistors

In contrast to nanoscale devices based on single or aligned arrays of nanotubes, CNT-TFTs consist of a randomly oriented network of nanotubes, which mitigates challenges associated with placing and aligning CNTs, but ultimately results in a reduction in channel performance in favor of lower costs. In a similar fashion to nanoscale transistors, TFTs consist of a semiconducting channel, conductive contact and gate electrodes, and an insulating dielectric layer. However, the applications for TFTs tend to be quite different from their nanoscale counterpart, largely due to the cost-performance trade-off. Whereas nanoscale, high-performance CNT-FETs are aimed at digital logic or 3D IC applications, TFTs are aimed at lower cost applications such as low- to medium-scale circuitry, wearable/flexible sensors, and displays [14].

TFTs can exist in many configurations with a range of diverse material combinations. Two common approaches for fabricating CNT-TFTs are highlighted in figure 4. The first approach involves the use of vacuum-based processing for many (if not all) of the device components (highlighted in figures 4(a)–(c)). Such devices

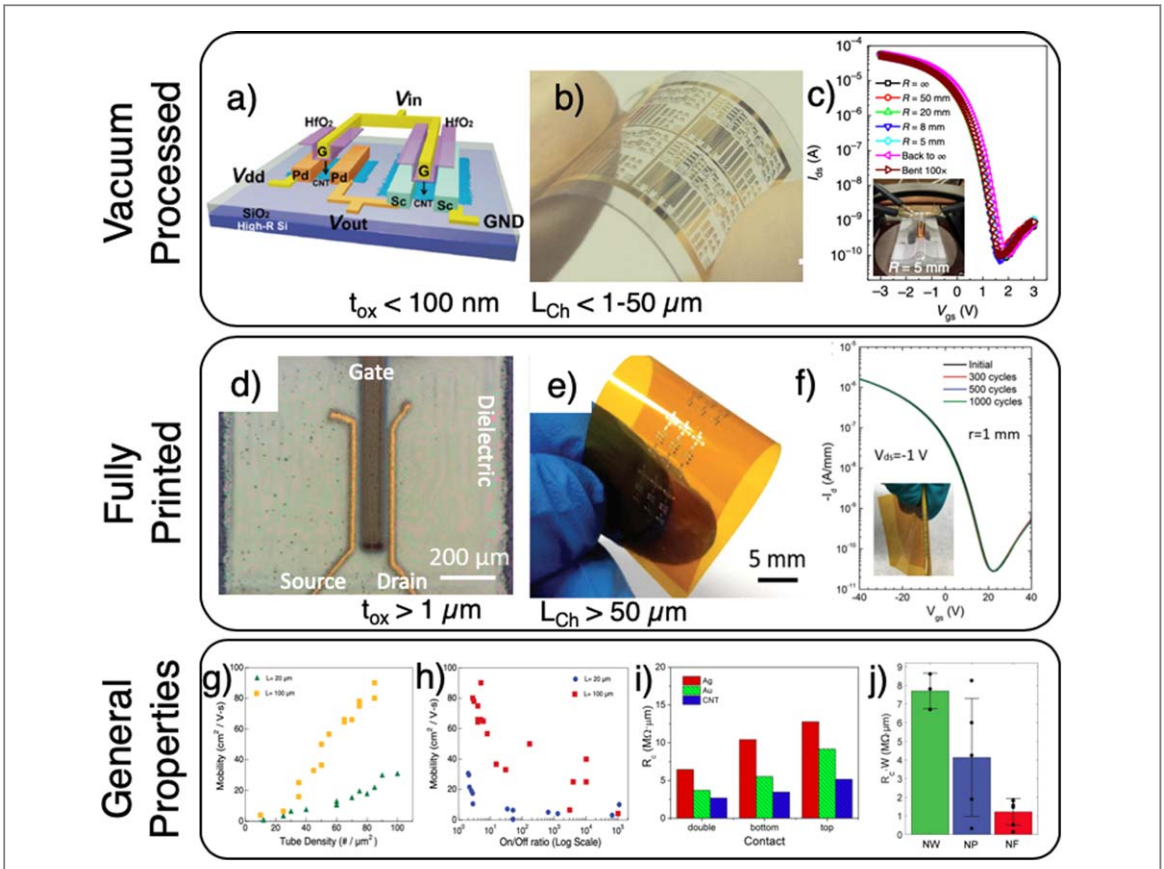

Figure 4. Outline of CNT-TFTs from different fabrication approaches, including their general characteristics. Representative (a) schematic, (b) picture, and (c) subthreshold characteristics of vacuum-processed CNT-TFTs. (a)–(c) Reproduced and adapted from [16, 24, 29], respectively. Representative (d) layout, (e) picture, and (f) subthreshold characteristics of fully printed CNT-TFTs with printed polymer dielectric. Reproduced and adapted from [92]. (g) Plot of proportional relationship between CNT-TFT mobility and CNT network density. (h) Plot of the inverse relationship between CNT-TFT mobility and I_{ON}/I_{OFF}. (g), (h) Reproduced and adapted from [91]. (i) Plot of the relationship between contact resistance and contact material/geometry. Reproduced and adapted from [71]. (j) Plot of the relationship between contact resistance and contact morphology. (i), (j) Reproduced and adapted from [69].

often consist of evaporated metal contacts and atomic layer deposition (ALD) grown dielectric layers and, in addition to these, there are often further steps with even greater complexity. The second approach is the printing of all device layers, as highlighted in figures 4(d)–(f), which typically produces devices that exhibit lower performance but can be fabricated at much lower cost. In general, however, the fundamental properties of the underlying CNT thin film remain the same, regardless of approach. As is highlighted in figure 4(g), as CNT network density is increased, channel mobility will increase proportionally. However, there often exists a trade-off between tube density, mobility, and on/off ratio, which is highlighted in figure 4(h) [91]. With regards to other device components, numerous approaches have been investigated in the fabrication of CNT-TFTs, many of which are summarized below, along with an outline of the relevant performance metrics associated with each process method.

The two predominant approaches for depositing contact metals are through evaporation or printing. For evaporation, typical contact materials include Pd or Au for achieving p-type transistor behavior. Although CNTs are intrinsic semiconductors, CNT transistors often exhibit p-type behavior due to a favorability for hole injection when using high-work function metals. One way to achieve n-type CNT transistors is to use low-work function contact metals, such as scandium or erbium, which favor electron injection [93, 94]. However, low-work function metals have a high propensity to oxidize, which necessitates immediate passivation and makes them difficult to process [31]. Additional methods for polarity conversions are covered in the following paragraphs. For printed contacts, silver nanoparticles are the most commonly used material due to their high conductivity, relatively low cost, and long-term performance stability [95]. However, a variety of printed contact materials have been demonstrated, including gold nanoparticles, metallic CNTs, various silver nanostructures, and eutectic gallium indium (liquid metal) [96]. Work carried out by Cao *et al* [71] showed that contact resistance to s-CNT films is directly related to contact material, with m-CNTs having the lowest contact resistance relative to Au and Ag nanoparticles. However, later work showed that the contact interface between Ag and s-CNTs can be improved by changing the particle morphology from nanoparticles to nanoflakes [69].

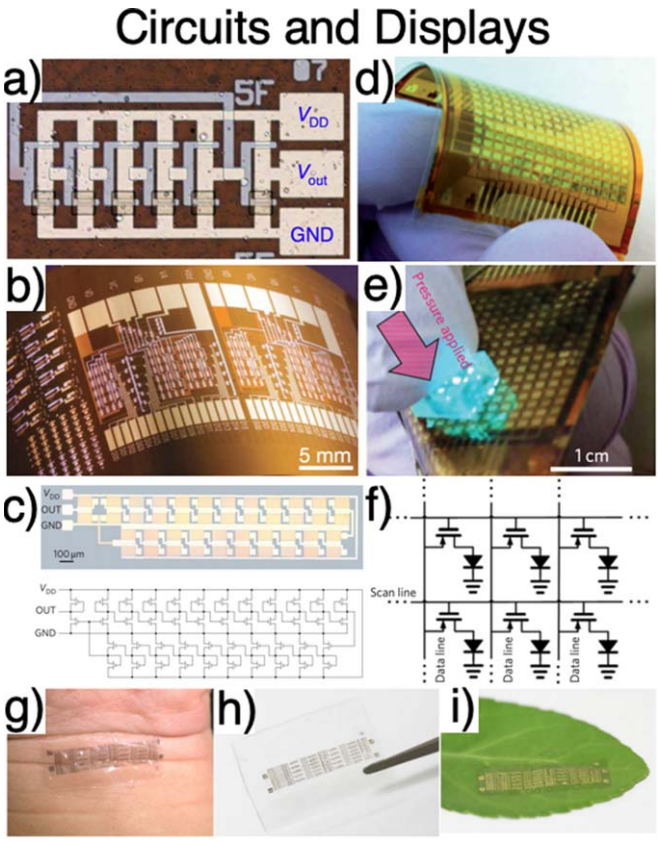

Figure 5. Overview of CNT-TFT circuit and display demonstrations. (a) Layout of a five-stage ring oscillator, which are frequently demonstrated in the CNT-TFT space to assess circuit speed. Reproduced and adapted from [24]. (b) Demonstration of more complex circuitry and integration schemes. Reproduced and adapted from [17]. (c) Layout and schematic of a 21-stage ring oscillator. Reproduced and adapted from [16]. (d), (e) Images of a flexible pressure sensitive display. (f) Schematic of the active matrix circuitry that is used in CNT-TFT display backplanes. (d)–(f) reproduced and adapted from [15]. (g)–(i) Images showing the bio-integration capabilities for transferable CNT-TFT circuits. Reproduced and adapted from [25].

With regards to dielectric layers, the ALD deposition of either Al_2O_3 or HfO_2 are two of the most common dielectrics from vacuum-based deposition [97–99]. Due to the fine control of layer thickness ($t_{ox} < 50$ nm), ALD oxides are capable of producing devices with small subthreshold swing (SS < 200 mV/dec) and low operating voltage ($V_{DD} < 5$ V). Additionally, oxide materials such as Al_2O_3 are capable of doping an underlying CNT layer and converting CNT-TFT operation to n-type [24]. However, in comparison to solution-processed polymer dielectrics, ALD oxides are less mechanically flexible and much more costly to deposit. Printed polymer oxides such as $BaTiO_3$/PMMA or PVP/pMSSQ composites have been shown to possess excellent flexibility and even stretchability while being compatible with solution processing and printing [100, 92, 101]. Even nanomaterial dielectrics, such as h-BN nanosheet networks, have shown promise [102]. However, the thickness of solution processable dielectrics are difficult to control and are susceptible to pinhole formation, potentially resulting in devices with low yield or poor uniformity. Alternatively, electrolyte-based dielectrics from ion gels have been shown to produce low-voltage devices while being compatible with solution processing [103, 104]. The advantages associated with ion gels are afforded by their unique polarization mechanism compared with simple dielectrics. Upon application of a gate voltage, mobile ions in the electrolyte accumulate at each electrode interface, giving rise to a double-layer capacitance that is on the order of 1–100 μF cm^{-2} that is independent of ion gel thickness [105]. Such large gate capacitance values enable ultra-low voltage operation. However, disadvantages associated with ion gels include slow polarization (switching) times and high gate leakage.

3.4. Circuits

While circuits have been realized from nanoscale (high-performance) CNT-FETs, they are less relevant for the majority of IoT application needs (as noted above). Hence, focus in this section is on circuits from the different types of CNT-TFTs. In order to execute more complex operations, CNT-TFTs have been widely utilized in a variety of circuit schemes. Although TFTs are not expected to overtake or replace commercial silicon ICs in digital processing applications, low- to medium-scale CNT-TFT-based circuitry can still be valuable for low-cost IoT applications. For instance, electronics involving RFID tags or standalone sensors may not require

Table 1. Benchmark comparison of the delay times for CNT-TFT based ring oscillators across various works. '—' indicates the metric was not reported in the original work.

Delay per stage (s)	V_{DD} (V)	Number of stages	Printed	Flexible	Year	Channel material	References
6.0e-6	15	15	No	Yes	2016	CNT	[109]
5.0e-6	6	51	No	No	2014	CNT	[110]
1.2e-6	2	5	Yes	Yes	2013	CNT	[103]
5.7e-9	17	5	No	Yes	2018	CNT	[24]
3.6e-10	1.9	5	No	No	2017	CNT	[106]
1.8e-11	2.8	5	No	No	2018	CNT	[108]
1.3e-11	1.5	—	No	No	1998	Silicon	[111]

powerful computing and can benefit from having low-cost, on-chip TFT circuitry. Despite the relatively small scale of CNT-TFT-based digital processing, much progress has been made toward the enabling of functional circuits suitable for IoT applications.

The simplest circuit element demonstrated throughout the CNT-TFT space is the inverter, whose function is to digitally invert a high input signal to a low output signal and vice versa. Inverters consist of two TFTs that can exist in a variety of configurations, but the three most common are complimentary inverters, ambipolar inverters, and unipolar inverters. For complimentary inverters, the input is tied to the gate of both an n-type and p-type TFT, and the output is tied to the drain of each device. Complimentary inverters are most desirable because of their steep voltage gain, minimal static power consumption, and tolerance to noise [29, 106]. However, it can be challenging to realize consistent n-type operation in CNT-TFTs, so many works have exploited the ambipolar characteristics of CNT-TFTs to create complimentary-like inverters [103, 107]. Still, these inverters exhibit negative trade-offs such as incomplete rail-to-rail output swings and high static power consumption. Finally, unipolar inverters consisting of a p-type depletion mode load [16, 108] are the simplest to fabricate; however, they cannot achieve zero-volt output-low signals, resulting in low voltage gains and high static power consumption.

Once inverters with reasonable transfer characteristics can be reliably fabricated, ring oscillators (ROs) can be used as a common test circuits, typically used to assess switching speed and overall circuit viability [109, 110]. ROs consist of an odd number of inverters cascaded into multiple stages so that the output of the previous inverter is tied to the input of the following inverter. An image of a five-stage RO consisting of complimentary CNT-TFT inverters is depicted in figure 5(a). An image of a larger 21-stage RO with unipolar inverters can be seen in figure 5(c) along with its schematic diagram. Table 1 outlines a comparison of the number of stages and delay times exhibited by CNT-TFT-based ROs across various works. Notably, Chen *et al* [110] have reported the largest scale CNT-TFT integration to-date, where they demonstrated 501-stage flexible ROs consisting of a hybrid integration of CNT-based p-TFTs and IGZO-based n-TFTs, with a total transistor count of 1002. As far as delay times, Peng and coworkers demonstrated ROs with stage delays as low as 18 ps [108], which are the fastest reported CNT-based ROs to-date, approaching speeds of silicon-based ROs [111].

Aside from test circuits, more complex functions have been achieved using CNT-TFTs, including NAND and NOR gates, sequential circuits, (D-latches, flip-flops, 4 bit adders), buffers, and amplifiers [16, 17, 99, 30]. Depicted in figure 5(b) is an image of a flexible chip containing such medium-scale circuitry, specifically a 4 bit row decoder containing up to 88 individual transistors. Jung *et al* [30] have used CNT-TFT-based circuitry (ROs, buffers and amplifiers) to drive fully printed flexible antennas and wireless sensor systems. Furthermore, due to the excellent stability and mechanical flexibility of carbon nanotube films, logic gates and sequential circuits on thin plastic films have been shown to be transferable onto biological surfaces such as a leaf or human skin (depicted in figures 5(g)–(i)) while maintaining high electrical performance [25].

3.5. Displays

Traditional commercial uses of TFT technologies have primarily come from the flat-panel display industry, where arrays of transistors are utilized in an active matrix (AM) to control the state of pixels, individually. Advantages of using an AM addressing scheme, in contrast to a passive matrix scheme, includes the minimization of signal cross-talk as well as superior spatial resolution and contrast. Current commercialized technologies rely on amorphous Si, polysilicon, or metal-oxide semiconductors (primarily indium gallium zinc oxide or IGZO), which have either limited mobility, poor stability, or suffer from high-fabrication cost [14, 112]. CNT-TFTs are promising devices within the realm of display technologies because of their high mobility, excellent stability and compatibility with low-cost fabrication (e.g. low-temperature, solution-based processing or printing).

A variety of works have already demonstrated CNT-TFT-based diode controllers and AM displays [15, 113, 114, 27], including fully printed display backplanes with pixel densities as high as 170 ppi [115]. As a further demonstration of complexity, CNT-TFT-based user-interactive displays have also been realized, which integrate an AMOLED display with pressure sensors to create an electronic skin with visual pressure feedback [15]. Ultimately, future work for CNT-TFT-based displays could involve a focus toward the development of low-cost, fully printed flexible displays that can be integrated with sensors onto clothes or human skin. Cao *et al* [26] have demonstrated such systems with the development of screen-printed electrochromic displays that can be laminated onto biological surfaces. Jung *et al* [30] demonstrated a similar electrochromic display integrated with a sensor and antenna. For future large-area applications, the solution-compatibility of CNTs and their freedom from vacuum-based processing methods can enable the development of meter-scale electronic wallpapers and interactive displays.

4. Carbon nanotube-based sensors

In combination with circuits and display electronics, carbon nanotubes have been used extensively in electronic sensors for applications including physical sensing, chemical sensing, and biological sensing. There are multiple reasons that CNTs provide an attractive electronic transduction platform for sensing, but the strongest motivations extend from their excellent mechanical and electrical properties [116–118] and their compatibility with low-cost fabrication schemes, such as printing [9, 92, 119, 120]. Recent advances in CNT synthesis, sorting, and placement strategies [33, 121, 122], along with the development of complex electronic devices such as field-effect transistors and TFTs [123, 124], have led to numerous sensing demonstrations. In this section, we highlight sensing demonstrations that utilize CNTs directly as the transduction platform for applications including pressure and strain sensors, chemical sensors, and biological sensors. All of the demonstrated applications are highly relevant for the IoT, as they enable the translation of real-world information to electronic signals that can be easily communicated using modern wireless technologies.

4.1. CNT-based physical sensors

Physical sensing is critical for many IoT applications. Pressure can provide information regarding the presence of an object, a user input, or even weather monitoring. Strain sensing can also be essential in measuring deformation, damage, or changes in ambient conditions like wind. Knowledge of such physical parameters can provide pathways to make data-informed decisions for preventative maintenance and can also provide a means for feedback-controlled actuators in robotic applications. This section of the review focuses primarily on sensing the formerly mentioned parameters (pressure and strain), however, temperature [125] and humidity [126, 127] sensors have also been demonstrated utilizing CNT transduction platforms and are important physical parameter sensing devices as well.

The purpose of strain sensing is to transduce mechanical deformation into a communicable signal. In the case of CNTs, mechanical deformation causes a change in their electrical properties, which can then be ascertained through electronic monitoring. The most common method of fabricating CNT-based strain sensors involves encapsulating a network of CNTs into a deformable composite (typically a polymeric elastomer) [128–130]. The change in the volumetric density of the CNTs due to a deformation of the composite material modulates the electronic parameters of the system, either in the form of altered resistance or altered capacitance.

An example of a capacitive-based strain sensor is shown in figures 6(a)–(d). In this work, carried out by Lipomi *et al* [19], two orthogonal stripes of conducting CNTs are separated by a thin layer of PDMS. The resulting sandwich structure is then fully encapsulated in PDMS. As the structure is stretched in either direction, the separation layer becomes thinner resulting in a capacitance change that is linearly correlated to strain. The fact that the separation layer is also deformable by pressure allows this same system to be used for pressure sensing. Lastly, due to the optical properties of CNT thin films, this sensor is able to be fully transparent.

An example of a resistive strain sensor is shown in figures 6(e)–(g). In this work, carried out by Takei *et al* [5], PDMS is coated on three sides with a conducting CNT and silver nanoparticle composite. On one of the long ends, as seen in figure 6(e), the composite contains a much smaller concentration of silver nanoparticles. Due to this composite structure, the resistance of one side of the whisker dominates the overall resistance of the structure. As the whisker is bent, the strain causes the composite to elongate and the resistance to increase. This is true for both tensile and compressive bending. The thin nature of the device makes it incredibly sensitive to small amounts of strain and can therefore be used to sense modulation in ambient air flow. Additionally, the whisker structure allows for spatial mapping of strain and could be used for robotic applications.

Many pressure sensors rely on the same operating mechanism of the capacitive and resistive strain sensors above. Mechanical deformation due to an external pressure modulates the resistivity of a carbon nanotube-based composite, or the thickness of a deformable elastomer, both leading to measurable changes in either

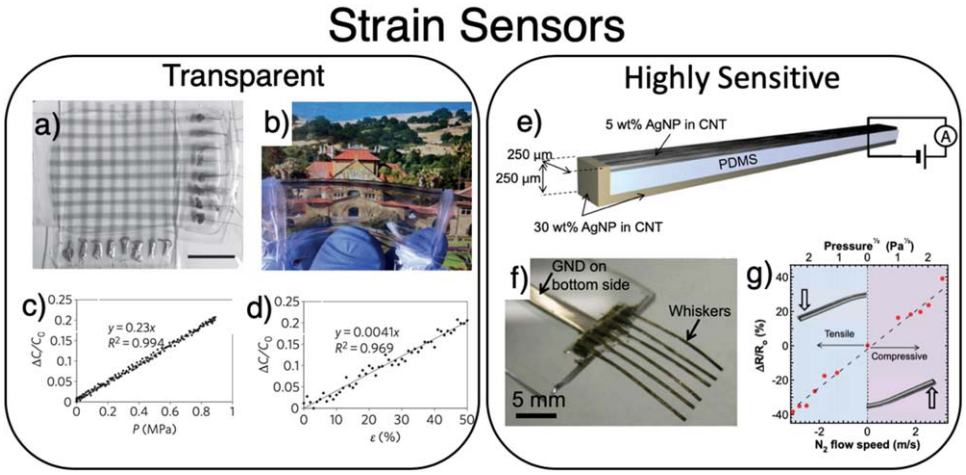

Figure 6. Strain sensors utilizing electronic CNT transduction. (a), (b) Photographs of an array of dual-layer compressible capacitive sensors. The sensor utilizes orthogonal stripes of unsorted single-walled nanotubes deposited in a method to induce buckling. The pressure response of the sensor is shown in (c) and the elongation response is presented in (d). (e) Schematic of a whisker-like strain sensor utilizing a CNT and Ag nanoparticle composite as a conductor with a strain-variable resistance. (f) A photograph of an array of 6 whisker sensors with the response to pressure induced by flowing nitrogen displayed in (g). (a)–(d) are adapted from [19] and (e)–(g) are adapted from [5].

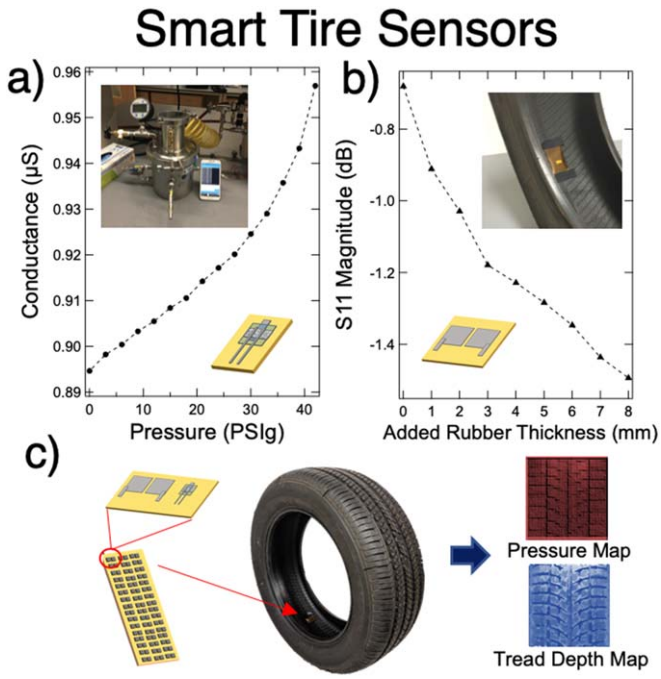

Figure 7. Fully printed, CNT-based smart tire sensing system. (a) The conductance versus environmental pressure of a printed CNT-TFT. The test is completed inside a pressure chamber and communicated via Bluetooth to a mobile phone. The insets include a photograph of the pressure chamber and a schematic of the device. (b) A printed Ag nanoparticle/CNT hybrid sensor capable of detecting tire rubber/tread thickness. The insets include a schematic of the device and a photograph of the sensor inside of a tire. (c) Conceptual schematic illustration of the capabilities of arrays of these sensors to map the pressure and tread from within an automobile tire. (a)–(c) are adapted from [136].

resistance or capacitance [131–133]. Overall, CNT-based sensors offer higher sensitivity when compared to traditional metal-foil strain gauges, but ultimately less consistent operation based on demonstrations to date [134].

A key challenge that faces CNT-based sensing devices is hysteretic operation. The friction that exists between solid-state conductors and soft materials leads to a nonuniform relaxation causing hysteretic behavior in both strain and pressure sensing. Additionally, as the composite structure is deformable by pressure/strain, the operation of the device can shift over time as the structure may experience changes after many relaxation cycles

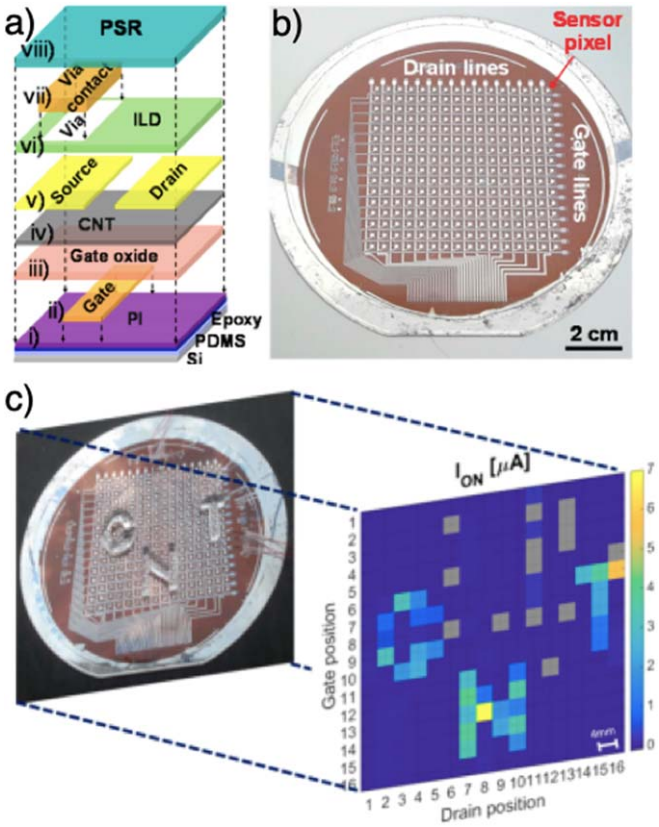

Figure 8. CNT transistors used to facilitate an active matrix pressure sensing array. (a) Layer structure of CNT-TFT connected to pressure-sensitive rubber. (b) Photograph of wafer-scale active matrix sensing array. (c) Demonstration of spatial mapping capability of the active matrix pressure sensor array. (a)–(c) are adapted from [28].

[135]. The low-cost fabrication and sensitivity of these devices, however, compels their use for IoT applications with less strict performance requirements.

One specific embodiment that has recently been demonstrated (and is a direct example of the impact CNT-based physical sensors can have on smart objects) is a smart tire system composed solely of CNT sensors. The system incorporates two sensing modalities—a CNT-TFT pressure sensor and a cross-capacitance material thickness sensor. The response of the sensors to automobile tire pressure and tire tread thickness are shown in figures 7(a), (b), respectively, while a conceptual schematic of the utility of the sensor system is in figure 7(c). The pressure sensor shows a direct modulation in conductance that is associated with changing environmental pressure [136]. This stems from the external air-pressure causing a deformation of either the carbon nanotube network, reducing the contact resistance between individual CNTs, or the printed dielectric, which increases the gate's electrostatic control of the channel. The tire tread thickness sensor works through two parallel CNT thin-film electrodes. An oscillating electric field is applied between the two electrodes and extends out-of-plane. This fringing field interacts with overlaid material, in this case tire tread, and the signal reflectance resulting from the fringing field is directly related to the material's thickness [20]. Ultimately, an array of both sensors could be used to develop a truly smart tire, in which a map of the pressure differentials and the tire tread thickness could be measured and communicated to the driver.

Along with CNTs and CNT-based materials being utilized for the transduction mechanism of pressure sensors, recent work has demonstrated promising results by utilizing CNT-TFTs to generate AM sensor arrays [15, 137, 138, 28]. In this scheme, an array of CNT-TFTs are placed in series with pressure-sensitive rubber (PSR). This serves two purposes: the transistor can act as an amplifier and transduce the modulating voltage from the PSR to a larger current for measurement purposes, and the transistor can be used to address a specific sensor in an array, similar to AM displays. An example of an AM sensor addressing scheme can be seen in figures 8(a)–(c). In this work, carried out by Nela *et al* [28], a wafer scale, flexible CNT-TFT matrix in conjunction with PSR is able to distinguish spatially distributed pressure. This is exemplified through the mapping of objects on the surface, a potentially interesting endeavor for IoT applications in detecting item location and weight.

For emerging large-area applications, printing CNT-TFT-based AM arrays is a promising route to realizing concepts such as electronic wallpapers and low-cost interactive displays, since printing is unrestricted by substrate size or vacuum-based deposition equipment. Roll to roll (R2R) printers, which can be as large as an

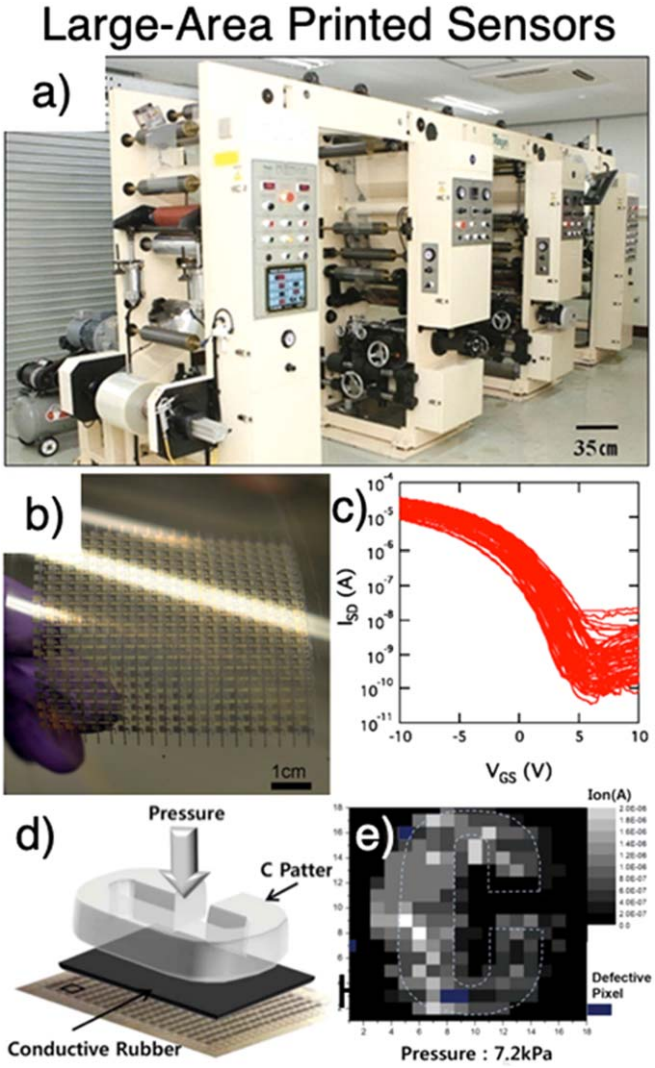

Figure 9. Overview of printed, large area, distributed sensors. (a) Image of a R2R gravure printer for high-throughput, large-area printing. Reproduced and adapted from [139]. (b) Image of an array of gravure-printed CNT-TFTs and (c) their subthreshold characteristics. (b), (c) Reproduced and adapted from [80]. (d) Demonstration of a distributed large-area gravure-printed pressure sensor based on a CNT-TFT active matrix and (e) a map of its output currents during applied pressure. Reproduced and adapted from [138].

entire room, as illustrated in figure 9(a), are best suited to produce large-area electronics, as these printers can be scaled up to printing throughputs on the order of tens of meters per second [139]. With regards to printing CNT-TFTs, works by Lau *et al* [80] have shown that distributed arrays of CNT-TFTs can be printed with high reproducibility and yield using R2R gravure printing methods, as demonstrated in figures 9(b), (c). Using distributed arrays of CNT-TFTs, large-area pressure sensing AM arrays have been fabricated using PSR, in a similar fashion as was outlined above [138].

4.2. CNT-based chemical sensors

One of the key advantages of an IoT infrastructure is consistent environmental monitoring to increase safety or allow for informed environmental conservation intervention. In these regards, the concentrations of specific molecular species within a gaseous or liquid environment are important parameters to monitor for many IoT applications. Carbon nanotube-based electrical devices have been used as chemical sensors since their conception [140, 141]. Due to their size scale and inherent electronic sensitivity, ambient analytes can have a measurable electrical effect on CNTs. In this sub-section, we present a brief overview of the mechanisms in which CNT-based devices can sense chemical analytes as well as highlight a few specific recent demonstrations. For a more comprehensive review on CNT-based chemical sensors, we recommend a recent work by Schroeder and coworkers [142].

The most prevalent types of electronic CNT chemical sensors utilize CNTs (either individual tubes or networks of CNTs) as resistors or transistors. For resistive elements, the chemical analyte modifies the

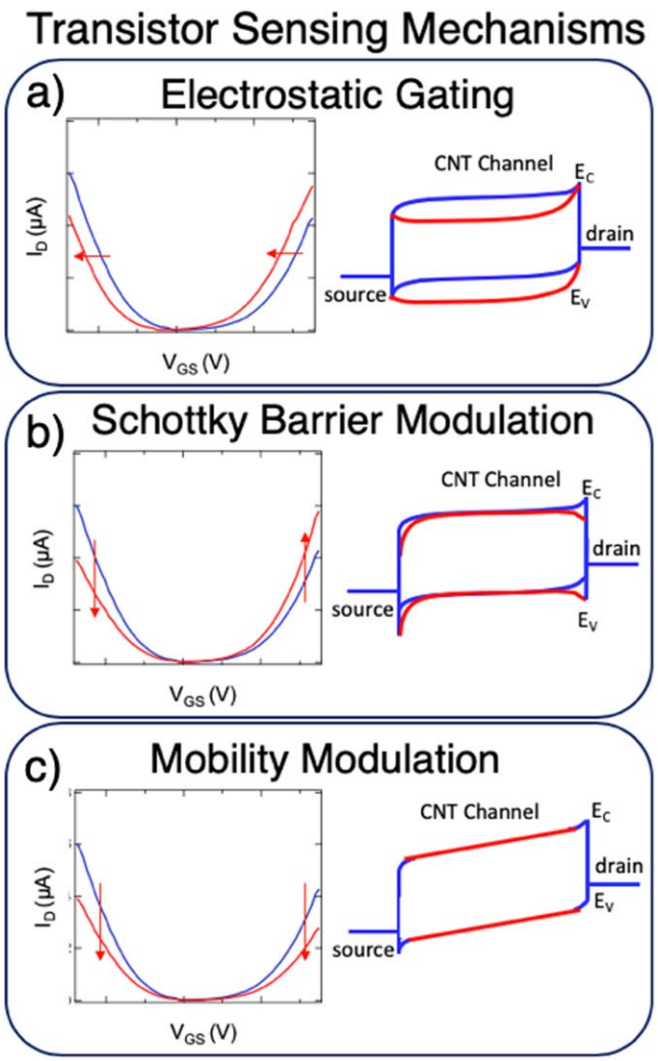

Figure 10. Sensing mechanisms of CNT-TFTs. Illustrated I_D–V_{GS} curves for three of the most prominent CNT sensing schemes. (a) Electrostatic gating in which proximate charge modulates the potential of the CNT channel. (b) Schottky barrier modulation in which the metal-CNT barrier potential is modulated. (c) Mobility degradation due to creation of defects or trapped charge states within a CNT channel.

conductivity of a single CNT, the interface of a CNT with another, or even the CNT-metal contact junction. The means of modification are many-fold but can include increasing the junction distance within a CNT network leading to increased inter-CNT resistance [143] or occupying trap states at defect sites to increase scattering [7]. Electrical measurements alone are not enough to allude to the mechanism of conductivity modification in resistive sensors, but other methods such as Raman or absorption spectroscopy can be used for elucidation.

On the other hand, transistor-based sensors have many different transduction mechanisms, which can be inferred from the current versus voltage characteristics [144]. The three primary methods of transduction include electrostatic gating [145, 146], Schottky barrier modulation [147, 148], and mobility modulation [149]. Illustrated *I*–*V* characteristics with subsequent band diagrams for each transduction mechanism can be seen in figures 10(a)–(c). For electrostatic gating, a charged analyte may approach the CNT by some distance shorter than the Debye screening length—defined as the largest distance a charge can be from a semiconductor to still have an appreciable effect on the surface potential. External charge acts as a gating entity to shift the valence/conduction bands with respect to the contact metal, thus modulating the Schottky barrier, which can be measured by a change in threshold voltage.

Another mechanism of CNT transistor-based transduction is Schottky barrier modulation. In this mechanism, electron/hole donating analytes may transfer charges directly to the nanotubes or to the contact metals to induce a change in electron/hole carrier density or the contact metal work function, measurable by opposing changes in both n- and p-branch carrier injection. The doping effect can also be gleaned from other methods apart from *I*–*V* characteristics, such as Raman spectroscopy. While both Schottky barrier modulation

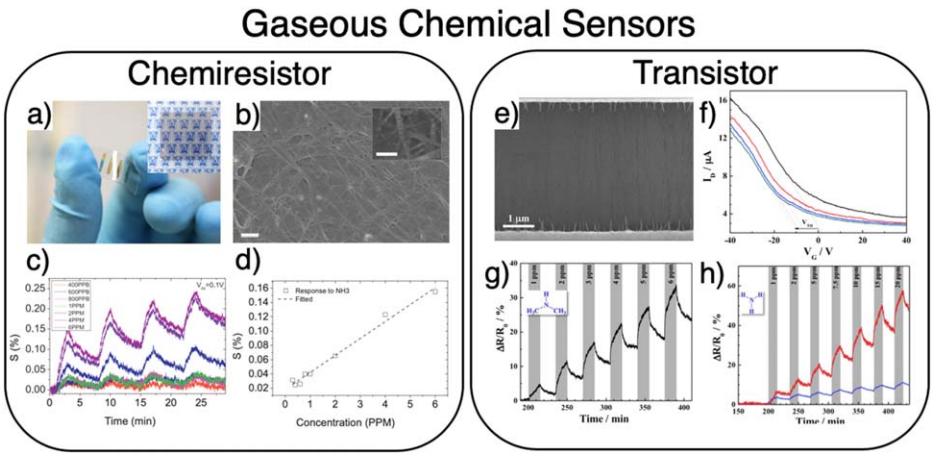

Figure 11. CNT-based gaseous chemical sensors. (a) Photograph of a flexible gold nanoparticle-functionalized CNT chemiresistor. (b) An SEM image of the chemiresistor CNT channel. The scale bar is 200 nm and inset scale bar is 100 nm. (c) The transient response of the sensor due to various concentrations of NH_3. The gas is periodically introduced for 2 min intervals beginning at 1 min and repeated every 7 min (d) The sensitivity with respect to concentration of NH_3 from 200 PPB to 6 PPM (e) SEM image of a parallel CNT transistor device for gas sensing. (f) The transfer characteristics of the parallel CNT transistor after functionalization with calixarene. The transistor was tested in air (black), NH_3 (red), DMA (blue), and TMA (green). (g), (h) the transient response of the sensor to both DMA and NH_3, respectively. The blue curve in (h) represents a transistor with no calixarene functionalization. Figures (a)–(d) are adapted from [157] and (e)–(h) are adapted from [158].

and electrostatic gating effects have been observed independently, it is also possible for sensitivity to be due to both Schottky barrier and electrostatic mechanisms happening in conjunction with each other [150].

The final illustrated effect, which is conceptually similar to how the resistive CNT chemical sensors function, is mobility modulation. For this mechanism, analytes absorb onto the CNTs and either induce carrier trapping or scattering. This mechanism is observed through a decrease in both the n- and p-branch current and manifests on a band diagram as the steepening of the band edge slopes from source to drain. Another mechanism that could be responsible for this behavior is capacitive coupling [151], which is rarer as it requires close to full coverage by the sensing analyte on the nanotube network or channel, but can be pictured as a continuous film separating the CNT from the gating mechanism, reducing electrostatic control and device transconductance [144].

To produce an effective chemical sensor, there are a few metrics that must be optimized, including the sensor's sensitivity and specificity. Because CNTs are inherently sensitive to many ambient conditions (e.g. humidity, various gasses, organic compounds), major challenges revolve around engineering devices to respond only to one specific analyte-selectivity. To overcome this obstacle, many functionalization methods have been studied, including organic polymer-based functionalization [152–154] and inorganic metal nanoparticle decoration [155, 156]. Each of these directions aim to: (1) provide binding sites for desired analytes and (2) incorporate functionalization entities that promote sensitivity.

Demonstrations of CNT-based gaseous sensors are highlighted in figure 11, specifically a resistivity-based sensor (figures 11(a)–(d)) [157] and a transistor-based sensor (figures 11(e)–(h)) [158]. The resistivity-based sensor consists of spray-coated CNTs decorated with Au nanoparticles on a transparent and flexible substrate (figure 11(b)). When exposed to ammonia (NH_3), the conductivity of the sensor is changed, as represented by their parameter for sensitivity—the change in resistance divided by the initial resistance. While CNT networks with no functionalization exhibit some sensitivity, that sensitivity is intensified with the addition of gold nanoparticles. This is due to the known mechanism of NH_3 gas modulating the metal work function of gold, thus modulating the Schottky barrier junction between the gold and the CNTs, which leads to a measurable change in overall resistance. This method has been shown to be recoverable and is linearly associated with NH_3 concentration. However, note that there is no inherent selectivity achieved in this NH_3 sensor as there are other gaseous species that could cause similar modulation.

The transistor-based sensor shown in figure 11(e) is composed of parallel CNTs, deposited from solution by dielectrophoretic alignment, between interdigitated gold electrodes and gated by a conducting substrate isolated by a 300 nm thick SiO_2 layer. The carbon nanotubes are functionalized by calixarene, a cyclic oligomer, to increase their affinity for binding with various nitrogen-based gas analytes. The sensor is shown to detect ammonia, and after a thorough analysis of the transistor characteristics, the sensing mechanism is concluded to be electrostatic gating due to the device exhibiting solely a threshold voltage shift with no modulation of the transconductance. In addition to sensing ammonia, the device proved a viable sensor for other amines, such as trimethylamine (TMA) and dimethylamine (DMA).

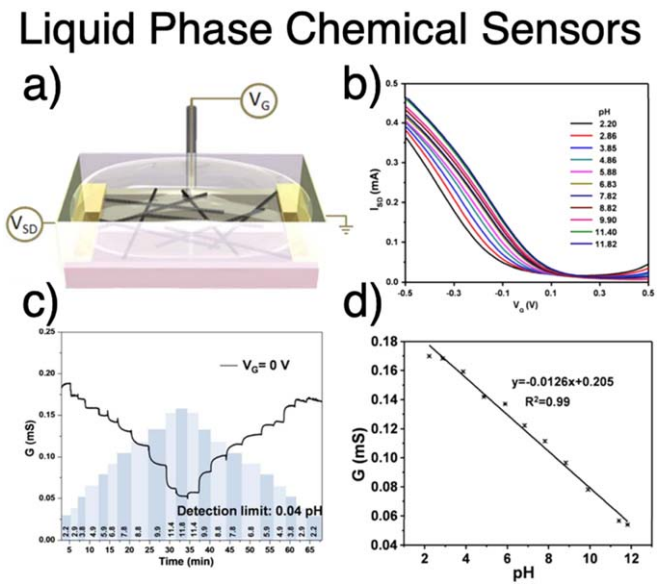

Figure 12. Poly(1-amino anthracene) functionalized CNT-TFT for pH sensing. (a) Schematic of the transistor device with solution-gating electrode. (b) Transfer curves of the device with respect to different pH in solution. (c) Transient response of the TFT at various pH under constant bias voltage. (d) Linear response of transconductance with respect to pH. (a)–(d) are adapted from [159].

Along with gaseous chemical sensors, CNTs have also been demonstrated as viable chemical sensors in liquid environments. In particular, CNT-TFTs functionalized with conductive polymers have proven adept at sensing pH in solution. The demonstration highlighted in figure 12 displays an ionically gated transistor in which the gating liquid's pH can be determined directly from the CNT-TFT's threshold voltage [159]. The device consists of semiconducting carbon nanotubes that are functionalized using a conducting polymer, poly (1-amino anthracene). A Ag/AgCl electrode is used to gate the device. As seen in the transistor curves, the threshold voltage shifts with increasing pH. This leads to a measurable change in conductance, which is shown in both figures 11(c) and (d). The range of the device is between pH levels of approximately 2 and 12. The sensor also shows a stable and recoverable response, as evident by the return to initial conductance levels after cycling the pH.

4.3. CNT-based biological sensors

The operation of CNT-based biological sensing is similar to that of chemical sensing, in which a desired analyte prompts a measurable change in the electronic properties of carbon nanotubes. This change can be measured through a CNT transistor's characteristics [144, 160, 161], the conductance of a CNT-based film [162, 163], or electrochemically [164–166]. The primary difference between CNT-based biological sensors (biosensors) and chemical sensors is in the functionalization needed and the environment of operation—with biosensors necessitating biorecognition elements and the ability to function in ionic, complex solutions. CNT-based sensors have provided many demonstrations of electronically transduced biosensors that have the potential to provide means for portable and even wearable diagnostics, leading to smarter and more ubiquitous healthcare through the IoT.

A successful biosensor necessitates two features—a biorecognition element and a transduction platform. The biorecognition element can vary drastically depending on the assay, but in general the categories can be separated into immunoassays (those relying on antibodies/synthetic aptamers) [160, 167, 168], enzymatic assays, and phenotype or genetic-based assays [169, 170]. CNTs offer an appropriately sensitive electronic transduction platform either through use as an electrode in an electrochemical cell, a resistor or resistive network, or a TFT. Additionally, recent works have demonstrated the ability to couple biorecognition elements to individual CNTs or to CNT networks through directly binding proteins to defect sites [171] or placing elements in proximity to CNTs through the utilization of polymer brushes [167]. Demonstrative examples of both electrochemical sensors utilizing CNT electrodes and immunoassays utilizing CNT-TFTs will be discussed below. For a more thorough discussion of CNTs used in biosensing applications, we recommend the review by Yang and coworkers [172].

For electrochemical sensing, carbon nanotube networks provide a high surface area electrode that can be functionalized with a biorecognition element, typically an enzyme. When an analyte is present, an enzymatic

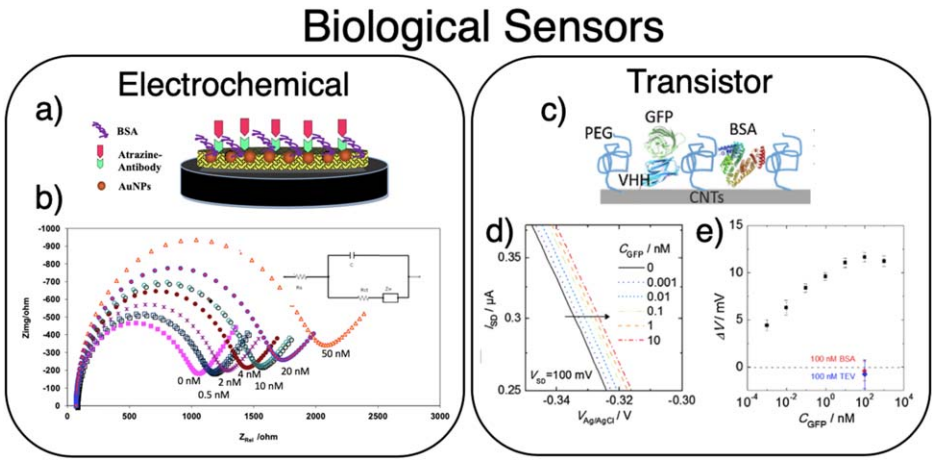

Figure 13. CNT-based biological sensors. (a) Multi-walled carbon nanotubes on a glassy carbon electrochemical cell that has been functionalized with atrazine antibodies. (b) Electrochemical response of the sensor under various concentrations of atrazine in PBS (pH = 7.0). (c) Schematic of a CNT-TFT that is functionalized with a polymer brush (PEG) and BSA molecules along with a biorecognition element VHH that is specific to GFP. (d) Transfer characteristics of the TFT under various concentrations of GFP. (e) Concentration dependence of the threshold voltage shift for GFP concentrations ranging from 1 pM to 1 μM. Figures (a), (b) are adapted from [173] and (c)–(e) are adapted from [167].

reaction produces an oxidizing or reducing reagent, which is measurable by cyclic voltammetry [164] or impedance spectroscopy [173]. An example of an electrochemical nanotube-based sensor that utilizes Au nanoparticle-functionalized multi-walled carbon nanotube electrodes can be seen in figure 13. The sensor is functionalized with an Atrazine antibody. If the analyte is present, it alters both the capacitance of the electrode and the electron transfer resistance. Through electrochemical impedance spectroscopy, one can then determine the concentration of atrazine in ionic solution, 1× phosphate-buffered solution. The outlook for this subset of electrochemical sensors is promising as the operation is robust, even in complex biological liquids, and CNTs offer a low-cost, high surface area electrode material that is biocompatible.

CNT transistor-based biosensors rely on the same mechanisms displayed in figure 10. A common CNT biosensor device consists of a field-effect transistor (either a single/parallel CNT device or a thin-film network) with antibodies or aptamers placed in direct proximity to the device. After the adsorption of tagged analytes, the proximate charge induces a measurable threshold voltage shift in the device [167]. One of the primary challenges with such a device is operation in ionic solutions [174]. The charges within the solution effectively screen detectable charges when they are outside the Debye length. To overcome this limitation some works have used shorter biorecognition elements, such as quarter-length aptamers [160], while others have developed methods of increasing the effective Debye length through surface functionalization [167, 175]. It has been found that through incorporating a polymer brush layer directly on top of the device, and embedding the biorecognition elements within that brush, effective devices that detect analytes in complex ionic solutions can be produced. An example of such a device is highlighted in figures 13(c)–(e). In this work, carried out by Filipiak *et al* [167], CNT-TFTs are functionalized with a polyethylene glycol (PEG) layer and nanobody receptors (VHH) are embedded in that layer. They find that with the PEGylated layer, they see a drastic increase in sensitivity in 100 mM Tris buffer solution using green florescent protein (GFP) as the model antigen. Overall, the polymer brush screens deleterious charges from the solution while allowing desired analytes to have a proximal effect on the electrostatics of the transistor.

More personalized, precise, and ubiquitous medicine necessitates biosensor devices that can transduce biological analytes and processes into communicable signals in a low-cost manner. Electronic transduction provides this means through avoiding expensive optical measurement components. Specifically, CNT-based devices that provide this electronic transduction platform show much promise for ushering low-cost and portable diagnostics into the IoT. Nevertheless, challenges do remain for the area of CNT-based biosensors. Despite decades of research effort and thousands of reports on a multiplicity of biosensors, no clear path exists for designing a CNT-based biological sensing platform. Many specific challenges can be cited as reasons for this lack of overall progress, but the primary issue is the lack of delivery on all needed performance metrics in a single approach/device. These metrics include: strong selectivity, high sensitivity, sufficient reproducibility, high yield, and operability in relevant biological milieu. While there have been many impressive demonstrations of CNT-based biosensors delivering on a few of these metrics, there has yet to be one that satisfies them all. What's more, often the solution for realizing one of the metrics will come at the cost of achieving another. Hence, going

forward, there must be focus on developing biosensors that can harness the advantages offered by CNTs while also delivering on all of the needed metrics for utility in real-world applications.

5. Challenges and outlook

5.1. Device-to-device uniformity

Although the CNTs in thin films are oriented in random directions, they can exhibit good uniformity and isotropy when the film is averaged out over a large area. However, many works have reported poor uniformity in devices between batches or runs when depositing or printing CNT networks from solution, especially when using drop-casting [176], spin-coating [177], or printing with unoptimized ink rheologies and surface chemistries [178]. For instance, poor ink rheology can produce an unwanted coffee ring effect during ink evaporation, resulting in poor film consistency [179]. These problems are exacerbated when scaling down device dimensions to length scales that are on the order of the CNTs themselves [112].

One of the primary factors associated with film uniformity is the deposition process. Methods such as substrate incubation or printing have been shown to produce highly uniform films, if the deposition parameters, solution rheology, and substrate surface chemistry have been carefully optimized. Dong *et al* [112] recently demonstrated a scalable method for producing highly uniform arrays of CNT films on 4 inch wafers and on large-area 0.37 m $\times$ 0.47 m backplane glass using the dip-coating method, which is a promising result for future display applications. Additionally, Rother and coworkers [75] have demonstrated a method for reproducibly aerosol jet printing CNT-TFTs with high-uniformity and for long periods of time by incorporating high-boiling point co-solvents to prevent nonuniform ink evaporation. With regards to printing and optimizing the uniformity of CNT films, it should also be noted that when fabricating CNT-based devices, the CNT films should be the first layer to be printed on a pristine substrate, as the presence of a previous layer during the CNT film rinsing step can result in solvent turbulence, giving rise to nonuniform channels across devices and chips [69].

5.2. Bias stress stability

The nature of the IoT demands devices and sensors that can operate for long periods of time without exhibiting excessive drift or degradation [180]. Sensor deployments in particular require stability in order for measurements to be meaningful. Unfortunately, the majority of published CNT sensor demonstrations are quick exhibitions that do not demonstrate or consider stability over time scales relevant to IoT deployments [181, 182]. In this section, we consider works that have explored stability over time periods up to several months, including observed shifts, decay modes, proper operating conditions, and proposed methods of increasing stability.

Many sensors in the IoT will experience periodic application and removal of voltages as the system powers up to send reports, while others will operate under a continuous bias as they monitor a value in near-real-time. From the perspective of stability, it is important to understand the consequences of long-term continuous bias or intermittent application and removal of voltages. Continuous operation of a CNT-FET composed of a few parallel nanotubes has been carried out in air for up to one week, as shown in figure 14(a) [13]. The majority of the week is composed of a stable regime, where fluctuations lead to coefficients of variation of approximately 5%. In this regime, no overall trend in drain current was observed. During the first few hours, however, drain current fell to nearly half of its initial value. Because the initial and final device characteristics are very similar (figure 14(b)), it is not likely that any permanent device degradation occurred, leading to the conclusion that the initial drop in drain current is likely due to changes in the occupancy of charge traps [183]. Despite this initial device settling not representing permanent degradation, the behavior could still present difficulties for deployed sensors, possibly requiring continuously operating sensors to wait for hours of stabilization before beginning to report meaningful data.

The settling effect just discussed also has bearing on sensors that power up periodically. When the gate voltage of a CNT device is swept or grounded, the settling period can be reset. As shown in figure 14(c), the drain current settling behavior can be observed repeatedly in this case. Ensuring that measurements always occur a fixed amount of time after the sensor is powered could be one method of combating this issue, but the strong rate of change of the drain current could lead to large variance. A pulsed voltage measurement approach may be the best solution in this case [186].

In addition to changes in the static drain current, many sensors are influenced by drift in other device metrics, such as the threshold voltage (V_{th}). The devices with parallel CNTs just discussed showed very little change in threshold voltage. Devices with thin-film networks of CNTs, however, have been shown to undergo large changes in threshold voltage as a result of gate bias stress (see figure 14(d)) [184, 187]. Further study is

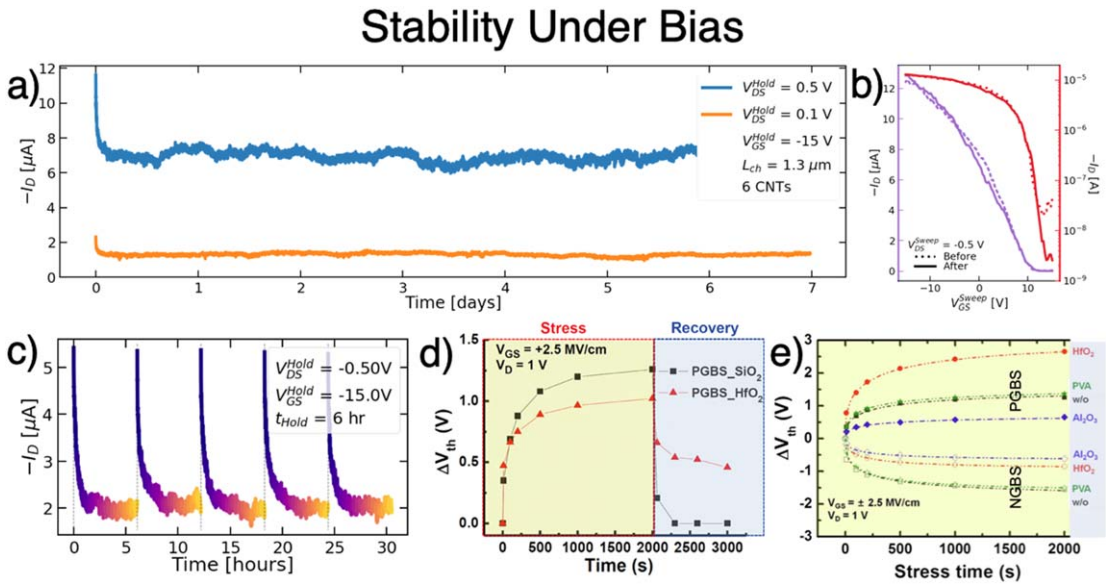

Figure 14. Stability of CNT transistors under continuous bias stress. (a) Stability is demonstrated for a device with 6 parallel CNTs under a moderate constant bias for a period of 7 d. (b) The switching characteristics of the device shown in the previous panel are very similar before and after the week-long bias stress. (c) The initial settling of drain current in long-term tests, also seen in (a), is shown to be a repeatable effect, likely due to changes in charge trap occupation over time. (d) For a CNT-TFT device, the primary effect of long-term bias stress is the threshold voltage shift shown here over time for the case of positive gate bias stress. (e) The effects of various passivation materials on the threshold voltage shift over bias stress time is shown, with some materials exaggerating the shift and others reducing the shift. Figures (a)–(c) are adapted from [13], (d) from [184], and (e) from [185].

warranted to determine whether this observed behavioral difference stems from the presence of CNT junctions or some other disparity between the particular devices studied.

Passivation of a CNT channel is the most commonly proposed method of removing device instabilities [185, 188]. While passivation can indeed have beneficial effects, it has been shown that threshold voltage shifts due to gate bias stress are still present with, and can even be exaggerated by, the passivation layer (see figure 14(e)) [189]. Because CNT-based sensors typically rely on interaction between nanotube and analyte, these sensors often either preclude the use of passivation materials entirely or severely limit the viable thickness range of the passivation material over the active sensing region of the carbon nanotube. As a result, passivation layers are capable of providing some benefits in certain situations, but do not comprise a ubiquitous solution to the instability challenge.

Any CNT sensor deployment must consider what voltage ranges are appropriate to use for the operating points of the device. It has long been known that as the drain to source voltage of a CNT device is increased in an environment that allows oxidation, eventually a breakdown voltage is reached where the nanotube is destroyed almost immediately ($\ll$1 s) [189, 190]. When CNT-based devices are operated for long periods of time, additional degradation modes become apparent that act on longer time scales. As the drain to source voltage is increased, the device has been found to pass from a stable mode to a slow decay mode, then a fast decay mode, finally reaching breakdown [13]. Current evidence suggests that devices could operate for very long periods of time (many months at least) when voltages target the stable regime. These operating regimes have been studied primarily in air on devices composed of parallel CNTs; more work is warranted to explore the effect of other relevant sensing environments and any differences that arise due to the junctions in devices composed of CNT network films.

Although some challenges still remain, the combination of passivation layers, pulsed voltage measurements, and use of operating voltages in the stable regime illuminates the start of the path toward robust CNT-based sensors with stability sufficient for IoT deployment. The demonstrated lack of net device degradation over periods of months provides a promising foundation for many IoT sensors with lifetimes on this order, and the lack of a degrading trend elicits positive implications for sensors that require lifetimes on the order of years. In cases where pulsed voltage measurements do not provide sufficiently stable sensor readings, proper choice of substrate material and further work exploring the reduction of substrate charge trapping could likely lead to adequate device stability.

5.3. Device type implications for sensing

Since sensors have been made using devices with random networks of CNTs, aligned CNTs, and single/few parallel CNTs, it remains to be addressed which device type is ideal for each type of sensor. In contrast to devices composed of randomly oriented CNT networks (which primarily have the advantage of simple and low-cost fabrication), increasing the alignment of CNTs in a network has been shown to improve both yield and device metrics such as mobility, off-current, and on/off ratio [191]. These improvements come at the cost of incorporating an alignment strategy into the fabrication process, although some alignment methods have been claimed to allow for industrial adoption [192]. Intrinsic device noise has also been shown to be greatly reduced with increasing CNT alignment, leading to a 4 order of magnitude reduction in the limit of detection of a demonstrated mercury sensor [193]. Many CNT chemical sensors measure the concentration of an analyte, with a current response that is proportional to that concentration. In this type of sensor, it is typically advantageous to have multiple CNTs, whether randomly oriented or aligned, composing the channel. For instance, a pH sensor has been shown to offer an additional order of magnitude of resolution when the channel is composed of many parallel CNTs as opposed to a single CNT [194].

A second type of sensor, referred to as 'single-molecule sensors,' have received increased research attention recently. Single-molecule sensors do not measure the concentration of an analyte by averaging many binding events, but instead monitor single molecule behavior over time. Examples include DNA sequencers [195], lysozyme behavior monitors [196], and molecular kinetics probes [197]. In sensors like these, only one monitored enzyme or molecule is bound per device, such that additional CNTs beyond the CNT with the binding site provide no benefit. In these cases, it is desirable to minimize the number of CNTs in a channel, preferably isolating a single semiconducting CNT as the channel for each device. Beyond the rough guidelines outlined here, the field could use further delineation of the cases in which random network, aligned, or single CNTs are ideal for sensing.

5.4. Comparison between CNTs and other thin-film semiconductors

This section briefly outlines the differences, advantages, and disadvantages associated with using CNT thin films and other thin-film semiconductors in transistor and circuit applications. Additional options for thin-film semiconductors include silicon (amorphous or polycrystalline), organics (such as P3HT or pentacene), oxides (such as IGZO), and 2D nanomaterials (such as MoS_2 or WSe_2). Both silicon and oxide-based thin-film semiconductors have found their way into commercial products in the flat-panel display industry, owed to their high performance, reliable fabrication and compatibility with traditional semiconductor-based manufacturing methods.

With regards to displays, amorphous silicon (a-Si) displays had a long-standing run as being state-of-the-art, due to their relatively low manufacturing cost and compatibility with liquid crystal display operation. However, a-Si mobilities lie in the range of 0.5–1 $cm^2\ V^{-1}\ s^{-1}$, which is prohibitively low for newer applications such as organic light emitting diode displays. For a period of time in the display industry, it was thought that a shift to low-temperature polysilicon, which has mobilities ranging from 30–300 $cm^2\ V^{-1}\ s^{-1}$, would have to be made. However, polysilicon's excessively high manufacturing costs prevents its widespread use. Eventually, indium gallium zinc oxide (IGZO), which has a higher mobility (1–100 $cm^2\ V^{-1}\ s^{-1}$) than a-Si, was adopted due to its similarity in processing to a-Si [198].

Looking forward in the display industry, many visions of future flat-panel display technologies include the increase in size of displays, increase in resolution, and development of new capabilities for flexible and extremely large-area applications. These goals call for the development of new materials and low-cost, vacuum-free processing methods. As has been outlined in previous sections, carbon nanotube thin films have great potential to enable emerging display technologies aligned with these visions, due to their commensurate mobility, low fabrication cost, as well as electrical and mechanical stability.

Aside from display applications, emerging IoT applications call for ubiquity. Such a vision also necessitates the use of low-cost fabrication and calls for flexible form factors. The primary material candidates for such applications are organics and carbon nanotubes. Although there have been flexible demonstrations of printed metal-oxide semiconductors, they typically require vacuum-processing methods, have prohibitively high processing temperatures, and/or are relatively inflexible [199]. In a similar fashion to CNTs, organic semiconductors are compatible with low-temperature solution processing and possess excellent flexibility in comparison to silicon and metal-oxide-based thin films. Historically, organics were the first printed semiconductors, which generated the advancement of printed electronics as a field and still have potential to enable printed optoelectronic applications, but their negative attributes preclude them from having a significant impact in TFT applications. These include their mobilities being quite low, typically $< 1\ cm^2\ V\ s$, resulting in low drive-current, and the fact that they suffer from poor ambient/electrical stability [200]. Printed nanotube films, in comparison, have mobilities that can range between 1 and 100 $cm^2\ V\ s$. Figure 15 outlines typical

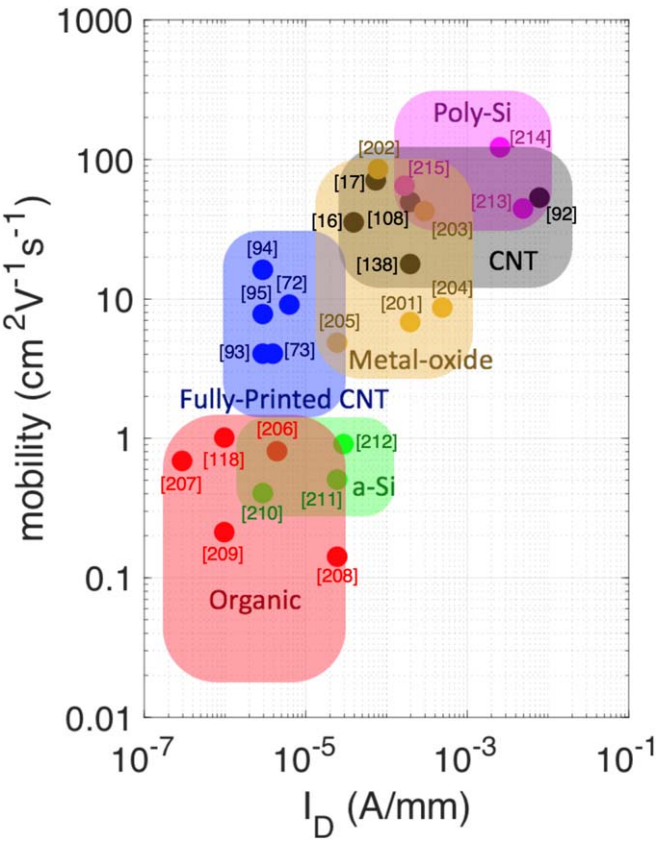

Figure 15. Overview of mobility versus drive current for TFTs consisting of various semiconducting channel materials (with $V_{DS} \leqslant 1$ V).

mobilities and drive-currents (with $V_{DS} \leqslant 1$ V) for each class of thin-film semiconductors [201–215]. However, it should be noted that the information in figure 15 is not exhaustive and drive currents are highly dependent on device geometries and gating / voltage bias schemes.

The emerging development of solution-processed 2D nanosheet networks (2DNNs) has created recent buzz in the field of printed semiconductors. However, it is uncertain if these materials will consistently exhibit the performance metrics, stability, and uniformity that established printed semiconductors have already achieved. Typical mobility values for 2DNNs are far less than that of a-Si [216]; however, there has been recent work demonstrating network mobilities as high as 10 cm^2 V s [217]. Mobilities as high as 91 cm^2 V s have been achieved using graphene networks but at the cost of low on/off ratio [102]. Further investigation of the reproducibility and stability of high-performance 2DNN is necessary as well as their demonstration in functional applications.

6. Conclusion

The emerging IoT ecosystem demands hardware consisting of reliable, low-cost materials capable of sustaining high electrical performance over long periods of time, yet sensitive enough to facilitate sensors that can consistently track changes in the surrounding environment. Carbon nanotubes have tremendous potential to enable the future of IoT systems, as evident from the vast array of already demonstrated circuits, sensors, and display electronics, many of which were fabricated using printing methods. Circuits consisting of carbon nanotubes possess the advantage of being mechanically flexible and low cost, with operating speeds approaching that of traditional silicon ICs. Meanwhile, the intrinsic sensitivity of CNTs, afforded by their nanoscale dimensionality and chemical properties, holds promise for enabling a variety of physical, chemical, and biological sensors. Additionally, many studies have shown that high CNT stability can be achieved for weeks on-end and performance variability can be quite low, given careful process optimization.

Moving forward, a variety of research directions can be pursued to expand the scope of CNT-based devices. For one, further exploiting the low-temperature process compatibility of CNTs can enable the development of extremely low-cost print-in-place circuitry, sensors, and displays, where the entire electronics production flow is carried out without removing the substrate from the printer. Another promising direction is the further

development of CNT-based biological sensors that rely on electronic transduction for point-of-care diagnostics. Ultimately, for thin-film-based devices, many issues associated with electrical stability must be addressed. Outside of device concepts, relatively little study has been devoted to challenges associated with proper encapsulation and packaging, which will be necessary before widespread use. Overall, due to the exceptional properties, compatibility with low-cost processing methods, and variety of already demonstrated electronics with high potential for future growth, we envision that CNT-based electronics can provide the backbone for the wireless sensor network infrastructure in the ongoing IoT revolution.

ORCID iDs

Jorge A Cardenas https://orcid.org/0000-0002-4403-8962
Joseph B Andrews https://orcid.org/0000-0002-3876-380X
Steven G Noyce https://orcid.org/0000-0002-2953-7560
Aaron D Franklin https://orcid.org/0000-0002-1128-9327

References

[1] Ashton K 2009 That 'Internet of Things' Thing *RFID J.* **22** 97–114
[2] Sundmaeker H, Guillemin P, Friess P and Woelfflé S 2010 *Vision and Challenges for Realising the Internet of Things* (Luxembourg: European Union) (https://doi.org/10.2759/26127)
[3] Gubbi J, Buyya R, Marusic S and Palaniswami M 2013 Internet of Things (IoT): a vision, architectural elements, and future directions *Future Gener. Comput. Syst.* **29** 1645–60
[4] Marinov V R 2015 Embedded flexible hybrid electronics for the Internet of Things *Int. Symp. Microelectron.* **1** 6–13
[5] Takei K, Yu Z, Zheng M, Ota H, Takahashi T and Javey A 2014 Highly sensitive electronic whiskers based on patterned carbon nanotube and silver nanoparticle composite films *Proc. Natl Acad. Sci.* **111** 1703–7
[6] Webb R C *et al* 2013 Ultrathin conformal devices for precise and continuous thermal characterization of human skin *Nat. Mater.* **12** 938–44
[7] Sharma S, Hussain S, Singh S and Islam S S 2014 MWCNT-conducting polymer composite based ammonia gas sensors: a new approach for complete recovery process *Sensors Actuators* B **194** 213–9
[8] Rosa P, Câmara A and Gouveia C 2015 *OJIOT* **1** 16–36
[9] Chen K *et al* 2016 Printed carbon nanotube electronics and sensor systems *Adv. Mater.* **28** 4397–414
[10] Dürkop T, Getty S A, Cobas E and Fuhrer M S 2004 Extraordinary mobility in semiconducting carbon nanotubes *Nano Lett.* **4** 35–9
[11] De Volder M F L, Tawfick S H, Baughman R H and Hart A J 2013 Carbon nanotubes: present and future commercial applications *Science* **339** 535–9
[12] Zhao Q, Gan Z and Zhuang Q 2002 Electrochemical sensors based on carbon nanotubes *Electroanalysis* **14** 1609–13
[13] Noyce S G, Doherty J L, Cheng Z, Han H, Bowen S and Franklin A D 2019 Electronic stability of carbon nanotube transistors under long-term bias stress *Nano Lett.* **19** 1460–6
[14] Franklin A D 2015 Nanomaterials in transistors: from high-performance to thin-film applications *Science* **349** aab2750
[15] Wang C *et al* 2013 User-interactive electronic skin for instantaneous pressure visualization *Nat. Mater.* **12** 899–904
[16] Sun D M *et al* 2011 Flexible high-performance carbon nanotube integrated circuits *Nat. Nanotechnol.* **6** 156–61
[17] Cao Q *et al* 2008 Medium-scale carbon nanotube thin-film integrated circuits on flexible plastic substrates *Nature* **454** 495–500
[18] Secor E B and Hersam M C 2015 Emerging carbon and post-carbon nanomaterial inks for printed electronics *J. Phys. Chem. Lett.* **6** 620–6
[19] Lipomi D J *et al* 2011 Skin-like pressure and strain sensors based on transparent elastic films of carbon nanotubes *Nat. Nanotechnol.* **6** 788–92
[20] Andrews J, Cao C, Brooke M and Franklin A 2017 Noninvasive material thickness detection by aerosol jet printed sensors enhanced through metallic carbon nanotube ink *IEEE Sens. J.* **17** 4612–8
[21] Kingery K 2017 Printed sensors monitor tire wear in real time (Accessed: 09 May, 2019) https://pratt.duke.edu/about/news/tread-sensor
[22] Honda W, Harada S, Arie T, Akita S and Takei K 2014 Wearable, human-interactive, health-monitoring, wireless devices fabricated by macroscale printing techniques *Adv. Funct. Mater.* **24** 3299–304
[23] Gao W *et al* 2016 Fully integrated wearable sensor arrays for multiplexed *in situ* perspiration analysis *Nature* **529** 509–14
[24] Tang J *et al* 2018 Flexible CMOS integrated circuits based on carbon nanotubes with sub-10 ns stage delays *Nat. Electron.* **1** 191–6
[25] Xiang L *et al* 2018 Low-power carbon nanotube-based integrated circuits that can be transferred to biological surfaces *Nat. Electron.* **1** 237–45
[26] Cao X *et al* 2016 Fully screen-printed, large-area, and flexible active-matrix electrochromic displays using carbon nanotube thin-film transistors *ACS Nano* **10** 9816–22
[27] Zhang J *et al* 2011 Separated carbon nanotube macroelectronics for active matrix organic light-emitting diode displays *Nano Lett.* **11** 4852–8
[28] Nela L, Tang J, Cao Q, Tulevski G and Han S-J 2018 Large-area high-performance flexible pressure sensor with carbon nanotube active matrix for electronic skin *Nano Lett.* **18** 2054–9
[29] Liu L *et al* 2019 Carbon nanotube complementary gigahertz integrated circuits and their applications on wireless sensor interface systems *ACS Nano* **13** 2526-2535
[30] Jung Y *et al* 2015 Fully printed flexible and disposable wireless cyclic voltammetry tag *Sci. Rep.* **5** 8105
[31] Franklin A D 2015 Carbon nanotube electronics *Emerging Nanoelectronic Devices* ed A Chen *et al* 1st edn (New York: Wiley) pp 315–35
[32] Hodge S A, Bayazit M K, Coleman K S and Shaffer M S P 2012 Unweaving the rainbow: a review of the relationship between single-walled carbon nanotube molecular structures and their chemical reactivity *Chem. Soc. Rev.* **41** 4409
[33] Arnold M S, Green A A, Hulvat J F, Stupp S I and Hersam M C 2006 Sorting carbon nanotubes by electronic structure using density differentiation *Nat. Nanotechnol.* **1** 60–5
[34] Wang H *et al* 2014 High-yield sorting of small-diameter carbon nanotubes for solar cells and transistors *ACS Nano* **8** 2609–17
[35] Gomulya W *et al* 2013 Semiconducting single-walled carbon nanotubes on demand by polymer wrapping *Adv. Mater.* **25** 2948–56
[36] Shi Z *et al* 1999 Mass-production of single-wall carbon nanotubes by arc discharge method *Carbon* **37** 1449–53

[37] Scott C D, Arepalli S, Nikolaev P and Smalley R E 2001 Growth mechanisms for single-wall carbon nanotubes in a laser-ablation process *Appl. Phys.* A **72** 573–80
[38] Kim K S, Cota-Sanchez G, Kingston C T, Imris M, Simard B and Soucy G 2007 Large-scale production of single-walled carbon nanotubes by induction thermal plasma *J. Phys. D.: Appl. Phys.* **40** 2375–87
[39] Kong J, Cassell A M and Dai H 1998 Chemical vapor deposition of methane for single-walled carbon nanotubes *Chem. Phys. Lett.* **292** 567–74
[40] Ma Y, Wang B, Wu Y, Huang Y and Chen Y 2011 The production of horizontally aligned single-walled carbon nanotubes *Carbon* **49** 4098–110
[41] Hu L, Hecht D S and Gruner G 2004 Percolation in transparent and conducting carbon nanotube networks *Nano Lett.* **4** 2513–7
[42] Ding L *et al* 2009 Selective growth of well-aligned semiconducting single-walled carbon nanotubes *Nano Lett.* **9** 800–5
[43] Patil N *et al* 2009 Wafer-scale growth and transfer of aligned single-walled carbon nanotubes *IEEE Trans. Nanotechnol.* **8** 498–504
[44] Döring V, Süss T and Hierold C 2014 Efficient transfer of carbon nanotubes for device fabrication using an LOR resist sacrificial layer *Sensors Actuators* A **208** 152–8
[45] Meitl M A *et al* 2006 Transfer printing by kinetic control of adhesion to an elastomeric stamp *Nat. Mater.* **5** 33–8
[46] Shulaker M M *et al* 2011 Linear increases in carbon nanotube density through multiple transfer technique *Nano Lett.* **11** 1881–6
[47] Wang H, Yuan Y, Wei L, Goh K, Yu D and Chen Y 2015 Catalysts for chirality selective synthesis of single-walled carbon nanotubes *Carbon* **81** 1–19
[48] Tulevski G S *et al* 2014 Toward high-performance digital logic technology with carbon nanotubes *ACS Nano* **8** 8730–45
[49] Franklin A D 2013 The road to carbon nanotube transistors *Nature* **498** 443–4
[50] Jin S H *et al* 2013 Using nanoscale thermocapillary flows to create arrays of purely semiconducting single-walled carbon nanotubes *Nat. Nanotechnol.* **8** 347–55
[51] Xie X *et al* 2014 Microwave purification of large-area horizontally aligned arrays of single-walled carbon nanotubes *Nat. Commun.* **5** 5332
[52] Ding L *et al* 2012 CMOS-based carbon nanotube pass-transistor logic integrated circuits *Nat. Commun.* **3** 677
[53] Ding L *et al* 2012 Carbon nanotube based ultra-low voltage integrated circuits: scaling down to 0.4 V *Appl. Phys. Lett.* **100** 263116
[54] Ryu K *et al* 2009 CMOS-analogous wafer-scale nanotube-on-insulator approach for submicrometer devices and integrated circuits using aligned nanotubes *Nano Lett.* **9** 189–97
[55] Shah K A and Tali B A 2016 Synthesis of carbon nanotubes by catalytic chemical vapour deposition: a review on carbon sources, catalysts and substrates *Mater. Sci. Semicond. Process.* **41** 67–82
[56] Liu H, Nishide D, Tanaka T and Kataura H 2011 Large-scale single-chirality separation of single-wall carbon nanotubes by simple gel chromatography *Nat. Commun.* **2** 309
[57] Tanaka T, Jin H, Miyata Y and Kataura H 2008 High-yield separation of metallic and semiconducting single-wall carbon nanotubes by agarose gel electrophoresis *Appl. Phys. Express* **1** 114001
[58] Nish A, Hwang J-Y, Doig J and Nicholas R J 2007 Highly selective dispersion of single-walled carbon nanotubes using aromatic polymers *Nat. Nanotechnol.* **2** 640–6
[59] Zheng M *et al* 2003 Structure-based carbon nanotube sorting by sequence-dependent DNA assembly *Science* **302** 1545–8
[60] Tang M S Y *et al* 2016 Metallic and semiconducting carbon nanotubes separation using an aqueous two-phase separation technique: a review *Nanotechnology* **27** 332002
[61] Janas D 2018 Towards monochiral carbon nanotubes: a review of progress in the sorting of single-walled carbon nanotubes *Mater. Chem. Front.* **2** 36–63
[62] Fagan J A, Becker M L, Chun J and Hobbie E K 2008 Length fractionation of carbon nanotubes using centrifugation *Adv. Mater.* **20** 1609–13
[63] Green A A, Duch M C and Hersam M C 2009 Isolation of single-walled carbon nanotube enantiomers by density differentiation *Nano Res.* **2** 69–77
[64] Cui J, Yang D, Zeng X, Zhou N and Liu H 2017 Recent progress on the structure separation of single-wall carbon nanotubes *Nanotechnology* **28** 452001
[65] Wang H and Bao Z 2015 Conjugated polymer sorting of semiconducting carbon nanotubes and their electronic applications *Nano Today* **10** 737–58
[66] Ding J *et al* 2015 A hybrid enrichment process combining conjugated polymer extraction and silica gel adsorption for high purity semiconducting single-walled carbon nanotubes (SWCNT) *Nanoscale* **7** 15741–7
[67] Samanta S K, Fritsch M, Scherf U, Gomulya W, Bisri S Z and Loi M A 2014 Conjugated polymer-assisted dispersion of single-wall carbon nanotubes: the power of polymer wrapping *Acc. Chem. Res.* **47** 2446–56
[68] Schießl S P *et al* 2017 Modeling carrier density dependent charge transport in semiconducting carbon nanotube networks *Phys. Rev. Mater.* **1** 046003
[69] Cardenas J A, Upshaw S, Williams N X, Catenacci M J, Wiley B J and Franklin A D 2019 Impact of morphology on printed contact performance in carbon nanotube thin-film transistors *Adv. Funct. Mater.* **29** 1805727
[70] Chung S, Cho K and Lee T 2019 Recent progress in inkjet-printed thin-film transistors *Adv. Sci.* **6** 1801445
[71] Cao C, Andrews J B, Kumar A and Franklin A D 2016 Improving contact interfaces in fully printed carbon nanotube thin-film transistors *ACS Nano* **10** 5221–9
[72] Wang C, Zhang J, Ryu K, Badmaev A, De Arco L G and Zhou C 2009 Wafer-scale fabrication of separated carbon nanotube thin-film transistors for display applications *Nano Lett.* **9** 4285–91
[73] Lee D *et al* 2014 High-performance thin-film transistors produced from highly separated solution-processed carbon nanotubes *Appl. Phys. Lett.* **104** 143508
[74] Tortorich R, Choi J-W, Tortorich R P and Choi J-W 2013 Inkjet printing of carbon nanotubes *Nanomaterials* **3** 453–68
[75] Rother M *et al* 2017 Aerosol-jet printing of polymer-sorted (6, 5) carbon nanotubes for field-effect transistors with high reproducibility *Adv. Electron. Mater.* **3** 1700080
[76] Williams N X, Noyce S, Cardenas J A, Catenacci M, Wiley B J and Franklin A D 2019 Silver nanowire inks for direct-write electronic tattoo applications *Nanoscale* (https://doi.org/10.1039/C9NR03378E)
[77] Cardenas J A, Catenacci M J, Andrews J B, Williams N X, Wiley B J and Franklin A D 2018 In-place printing of carbon nanotube transistors at low temperature *ACS Appl. Nano Mater.* **1** 1863–1869
[78] Metters J P, Gomez-Mingot M, Iniesta J, Kadara R O and Banks C E 2013 The fabrication of novel screen printed single-walled carbon nanotube electrodes: electroanalytical applications *Sensors Actuators* B **177** 1043–52
[79] Koo H *et al* 2015 Scalability of carbon-nanotube-based thin film transistors for flexible electronic devices manufactured using an all roll-to-roll gravure printing system *Sci. Rep.* **5** 14459
[80] Lau P H *et al* 2013 Fully printed, high performance carbon nanotube thin-film transistors on flexible substrates *Nano Lett.* **13** 3864–9

[81] Homenick C M *et al* 2016 Fully printed and encapsulated SWCNT-based thin film transistors via a combination of R2R gravure and inkjet printing *ACS Appl. Mater. Interfaces* **8** 27900–10
[82] Qiu C, Zhang Z, Xiao M, Yang Y, Zhong D and Peng L-M 2017 Scaling carbon nanotube complementary transistors to 5-nm gate lengths *Science* **355** 271–6
[83] Franklin A D *et al* 2012 Sub-10 nm carbon nanotube transistor *Nano Lett.* **12** 758–62
[84] Shulaker M M *et al* 2013 Carbon nanotube computer *Nature* **501** 526–30
[85] Rutherglen C and Burke P 2007 Carbon nanotube radio *Nano Lett.* **7** 3296–9
[86] Steiner M *et al* 2012 High-frequency performance of scaled carbon nanotube array field-effect transistors *Appl. Phys. Lett.* **101** 053123
[87] Kang S J *et al* 2007 High-performance electronics using dense, perfectly aligned arrays of single-walled carbon nanotubes *Nat. Nanotechnol.* **2** 230–6
[88] Graham A P *et al* 2005 How do carbon nanotubes fit into the semiconductor roadmap? *Appl. Phys.* A **80** 1141–51
[89] Salahuddin S, Ni K and Datta S 2018 The era of hyper-scaling in electronics *Nat. Electron.* **1** 442–50
[90] Shulaker M M *et al* 2017 Three-dimensional integration of nanotechnologies for computing and data storage on a single chip *Nature* **547** 74–8
[91] Rouhi N, Jain D, Zand K and Burke P J 2011 Fundamental limits on the mobility of nanotube-based semiconducting inks *Adv. Mater.* **23** 94–9
[92] Cao C, Andrews J B and Franklin A D 2017 Completely printed, flexible, stable, and hysteresis-free carbon nanotube thin-film transistors via aerosol jet printing *Adv. Electron. Mater.* **3** 1700057
[93] Zhang Z *et al* 2007 Doping-free fabrication of carbon nanotube based ballistic CMOS devices and circuits *Nano Lett.* **7** 3603–7
[94] Shahrjerdi D, Franklin A D, Oida S, Ott J A, Tulevski G S and Haensch W 2013 High-performance air-stable n-type carbon nanotube transistors with erbium contacts *ACS Nano* **7** 8303–8
[95] Rajan K, Roppolo I, Chiappone A, Bocchini S, Perrone D and Chiolerio A 2016 Silver nanoparticle ink technology: state of the art *Nanotechnol. Sci. Appl.* **9** 1–13
[96] Andrews J B *et al* 2018 Patterned liquid metal contacts for printed carbon nanotube transistors *ACS Nano* **12** 5482–8
[97] Geier M L *et al* 2015 Solution-processed carbon nanotube thin-film complementary static random access memory *Nat. Nanotechnol.* **10** 944–8
[98] Kim B, Geier M L, Hersam M C and Dodabalapur A 2017 Inkjet printed circuits based on ambipolar and p-type carbon nanotube thin-film transistors *Sci. Rep.* **7** 39627
[99] Yang Y, Ding L, Han J, Zhang Z and Peng L-M 2017 High-performance complementary transistors and medium-scale integrated circuits based on carbon nanotube thin films *ACS Nano* **11** 4124–32
[100] Cai L, Zhang S, Miao J, Yu Z and Wang C 2016 Fully printed stretchable thin-film transistors and integrated logic circuits *ACS Nano* **10** 11459–68
[101] Cao X *et al* 2014 Screen printing as a scalable and low-cost approach for rigid and flexible thin-film transistors using separated carbon nanotubes *ACS Nano* **8** 12769–76
[102] Carey T *et al* 2017 Fully inkjet-printed two-dimensional material field-effect heterojunctions for wearable and textile electronics *Nat. Commun.* **8** 1202
[103] Ha M *et al* 2013 Aerosol jet printed, low voltage, electrolyte gated carbon nanotube ring oscillators with sub-5 μs stage delays *Nano Lett.* **13** 954–60
[104] Ha M *et al* 2010 Printed, sub-3V digital circuits on plastic from aqueous carbon nanotube inks *ACS Nano* **4** 4388–95
[105] Nketia-Yawson B and Noh Y-Y 2018 Recent progress on high-capacitance polymer gate dielectrics for flexible low-voltage transistors *Adv. Funct. Mater.* **28** 1802201
[106] Han S-J *et al* 2017 High-speed logic integrated circuits with solution-processed self-assembled carbon nanotubes *Nat. Nanotechnol.* **12** 861–5
[107] Kim B, Geier M L, Hersam M C and Dodabalapur A 2015 Inkjet printed circuits on flexible and rigid substrates based on ambipolar carbon nanotubes with high operational stability *ACS Appl. Mater. Interfaces* **7** 27654–60
[108] Zhong D *et al* 2018 Gigahertz integrated circuits based on carbon nanotube films *Nat. Electron.* **1** 40–5
[109] Zhao Y *et al* 2016 Three-dimensional flexible complementary metal-oxide-semiconductor logic circuits based on two-layer stacks of single-walled carbon nanotube networks *ACS Nano* **10** 2193–202
[110] Chen H, Cao Y, Zhang J and Zhou C 2014 Large-scale complementary macroelectronics using hybrid integration of carbon nanotubes and IGZO thin-film transistors *Nat. Commun.* **5** 4097
[111] Yang S *et al* 1998 A high performance 180 nm generation logic technology *Int. Electron Devices Meeting 1998. Technical Digest* pp 197–200
[112] Dong G *et al* 2018 Large-area and highly uniform carbon nanotube film for high-performance thin film transistors *Nano Res.* **11** 4356–67
[113] Chen P *et al* 2011 Fully printed separated carbon nanotube thin film transistor circuits and its application in organic light emitting diode control *Nano Lett.* **11** 5301–8
[114] Ishikawa F N *et al* 2009 Transparent electronics based on transfer printed aligned carbon nanotubes on rigid and flexible substrates *ACS Nano* **3** 73–9
[115] Li H, Tang Y, Guo W, Liu H, Zhou L and Smolinski N 2016 Polyfluorinated electrolyte for fully printed carbon nanotube electronics *Adv. Funct. Mater.* **26** 6914–20
[116] Ebbesen T W, Lezec H J, Hiura H, Bennett J W, Ghaemi H F and Thio T 1996 Electrical conductivity of individual carbon nanotubes *Nature* **382** 54–6
[117] Charlier J-C, Blase X and Roche S 2007 Electronic and transport properties of nanotubes *Rev. Mod. Phys.* **79** 677–732
[118] Salvetat J-P *et al* 1999 Mechanical properties of carbon nanotubes *Appl. Phys.* A **69** 255–60
[119] Fukuda K *et al* 2014 Fully-printed high-performance organic thin-film transistors and circuitry on one-micron-thick polymer films *Nat. Commun.* **5** 4147
[120] Park S, Vosguerichian M and Bao Z 2013 A review of fabrication and applications of carbon nanotube film-based flexible electronics *Nanoscale* **5** 1727
[121] Liyanage L S *et al* 2012 Wafer-scale fabrication and characterization of thin-film transistors with polythiophene-sorted semiconducting carbon nanotube networks *ACS Nano* **6** 451–8
[122] Kusaba M and Tsunawaki Y 2006 Production of single-wall carbon nanotubes by a XeCl excimer laser ablation *Thin Solid Films* **506–507** 255–8
[123] Tans S J, Verschueren A R M and Dekker C 1998 Room-temperature transistor based on a single carbon nanotube *Nature* **393** 49–52

[124] Snow E S, Campbell P M, Ancona M G and Novak J P 2005 High-mobility carbon-nanotube thin-film transistors on a polymeric substrate *Appl. Phys. Lett.* **86** 033105
[125] Sibinski M, Jakubowska M, Sloma M, Sibinski M, Jakubowska M and Sloma M 2010 Flexible temperature sensors on fibers *Sensors* **10** 7934–46
[126] Han J-W, Kim B, Li J and Meyyappan M 2012 Carbon nanotube based humidity sensor on cellulose paper *J. Phys. Chem.* C **116** 22094–7
[127] Yoo K-P, Lim L-T, Min N-K, Lee M J, Lee C J and Park C-W 2010 Novel resistive-type humidity sensor based on multiwall carbon nanotube/polyimide composite films *Sensors Actuators* B **145** 120–5
[128] Yamada T *et al* 2011 A stretchable carbon nanotube strain sensor for human-motion detection *Nat. Nanotechnol.* **6** 296–301
[129] Cai L *et al* 2013 Super-stretchable, transparent carbon nanotube-based capacitive strain sensors for human motion detection *Sci. Rep.* **3** 3048
[130] Shin M K, Oh J, Lima M, Kozlov M E, Kim S J and Baughman R H 2010 Elastomeric conductive composites based on carbon nanotube forests *Adv. Mater.* **22** 2663–7
[131] Tee B C-K *et al* 2015 A skin-inspired organic digital mechanoreceptor *Science* **350** 313–6
[132] Wang X, Li T, Adams J and Yang J 2013 Transparent, stretchable, carbon-nanotube-inlaid conductors enabled by standard replication technology for capacitive pressure, strain and touch sensors *J. Mater. Chem.* A **1** 3580
[133] Gerlach C *et al* 2015 'Printed MWCNT-PDMS-composite pressure sensor system for plantar pressure monitoring in ulcer prevention *IEEE Sens. J.* **15** 3647–56
[134] Siddall G and Smith G 1959 A thin film resistor for measuring strain *Vacuum* **9** 144–6
[135] Choi D Y *et al* 2017 'Highly stretchable, hysteresis-free ionic liquid-based strain sensor for precise human motion monitoring *ACS Appl. Mater. Interfaces* **9** 1770–80
[136] Andrews J B, Cardenas J A, Lim C J, Noyce S G, Mullett J and Franklin A D 2018 Fully printed and flexible carbon nanotube transistors for pressure sensing in automobile tires *IEEE Sens. J.* **18** 7875–80
[137] Takahashi T, Takei K, Gillies A G, Fearing R S and Javey A 2011 Carbon nanotube active-matrix backplanes for conformal electronics and sensors *Nano Lett.* **11** 5408–13
[138] Yeom C, Chen K, Kiriya D, Yu Z, Cho G and Javey A 2015 Large-area compliant tactile sensors using printed carbon nanotube active-matrix backplanes *Adv. Mater.* **27** 1561–6
[139] Noh J *et al* 2010 Scalability of roll-to-roll gravure-printed electrodes on plastic foils *IEEE Trans. Electron Packag. Manuf.* **33** 275–83
[140] Kong J *et al* 2000 Nanotube molecular wires as chemical sensors *Science* **287** 622–5
[141] Collins P G, Bradley K, Ishigami M and Zettl A 2000 Extreme oxygen sensitivity of electronic properties of carbon nanotubes *Science* **287** 1801–4
[142] Schroeder V, Savagatrup S, He M, Lin S and Swager T M 2019 Carbon nanotube chemical sensors *Chem. Rev.* **119** 599–663
[143] Niu L, Luo Y and Li Z 2007 A highly selective chemical gas sensor based on functionalization of multi-walled carbon nanotubes with poly(ethylene glycol) *Sensors Actuators* B **126** 361–7
[144] Heller I, Janssens A M, Männik J, Minot E D, Lemay S G and Dekker C 2008 Identifying the mechanism of biosensing with carbon nanotube transistors *Nano Lett.* **8** 591–5
[145] Roberts M E, LeMieux M C and Bao Z 2009 Sorted and aligned single-walled carbon nanotube networks for transistor-based aqueous chemical sensors *ACS Nano* **3** 3287–93
[146] Artyukhin A B, Stadermann M, Friddle R W, Stroeve P, Bakajin O and Noy A 2006 Controlled electrostatic gating of carbon nanotube FET devices *Nano Lett.* **6** 2080–5
[147] Zhang J, Boyd A, Tselev A, Paranjape M and Barbara P 2006 Mechanism of NO_2 detection in carbon nanotube field effect transistor chemical sensors *Appl. Phys. Lett.* **88** 123112
[148] Peng N, Zhang Q, Chow C L, Tan O K and Marzari N 2009 Sensing mechanisms for carbon nanotube based NH_3 gas detection *Nano Lett.* **9** 1626–30
[149] Wang F, Gu H and Swager T M 2008 Carbon nanotube/polythiophene chemiresistive sensors for chemical warfare agents *J. Am. Chem. Soc.* **130** 5392–3
[150] Liu X, Luo Z, Han S, Tang T, Zhang D and Zhou C 2005 Band engineering of carbon nanotube field-effect transistors via selected area chemical gating *Appl. Phys. Lett.* **86** 243501
[151] Chen R J *et al* 2003 Noncovalent functionalization of carbon nanotubes for highly specific electronic biosensors *Proc. Natl Acad. Sci.* **100** 4984–9
[152] Wei L *et al* 2014 Highly sensitive detection of trinitrotoluene in water by chemiresistive sensor based on noncovalently amino functionalized single-walled carbon nanotube *Sensors Actuators* B **190** 529–34
[153] Zhao Y-L, Hu L, Stoddart J F and Grüner G 2008 Pyrenecyclodextrin-decorated single-walled carbon nanotube field-effect transistors as chemical sensors *Adv. Mater.* **20** 1910–5
[154] Frazier K M and Swager T M 2013 Robust cyclohexanone selective chemiresistors based on single-walled carbon nanotubes *Anal. Chem.* **85** 7154–8
[155] Kong J, Chapline M G and Dai H 2001 Functionalized carbon nanotubes for molecular hydrogen sensors *Adv. Mater.* **13** 1384–6
[156] Sun Y and Wang H H 2007 High-performance, flexible hydrogen sensors that use carbon nanotubes decorated with palladium nanoparticles *Adv. Mater.* **19** 2818–23
[157] Lee K *et al* 2013 Highly sensitive, transparent, and flexible gas sensors based on gold nanoparticle decorated carbon nanotubes *Sensors Actuators* B **188** 571–5
[158] Sarkar T, Ashraf P M, Srinives S and Mulchandani A 2018 Calixarene-functionalized single-walled carbon nanotubes for sensitive detection of volatile amines *Sensors Actuators* B **268** 115–22
[159] Gou P *et al* 2015 Carbon nanotube chemiresistor for wireless pH sensing *Sci. Rep.* **4** 4468
[160] Kim J P, Lee B Y, Hong S and Sim S J 2008 Ultrasensitive carbon nanotube-based biosensors using antibody-binding fragments *Anal. Biochem.* **381** 193–8
[161] Pandana H, Aschenbach K H, Lenski D R, Fuhrer M S, Khan J and Gomez R D 2008 A versatile biomolecular charge-based sensor using oxide-gated carbon nanotube transistor arrays *IEEE Sens. J.* **8** 655–60
[162] Rajesh V, Sharma N K, Puri R K, Singh A M, Biradar and Mulchanadani A 2013 Label-free detection of cardiac troponin-I using gold nanoparticles functionalized single-walled carbon nanotubes based chemiresistive biosensor *Appl. Phys. Lett.* **103** 203703
[163] Gong J-L, Sarkar T, Badhulika S and Mulchandani A 2013 Label-free chemiresistive biosensor for mercury (II) based on single-walled carbon nanotubes and structure-switching DNA *Appl. Phys. Lett.* **102** 013701

[164] Quintero-Jaime A F, Berenguer-Murcia Á, Cazorla-Amorós D and Morallón E 2019 Carbon nanotubes modified with Au for electrochemical detection of prostate specific antigen: effect of Au nanoparticle size distribution *Front. Chem.* **7** 147
[165] Chen J, Zhang W-D and Ye J-S 2008 Nonenzymatic electrochemical glucose sensor based on MnO2/MWNTs nanocomposite *Electrochem. Commun.* **10** 1268–71
[166] Jacobs C B, Peairs M J and Venton B J 2010 Review: Carbon nanotube based electrochemical sensors for biomolecules *Anal. Chim. Acta* **662** 105–27
[167] Filipiak M S *et al* 2018 Highly sensitive, selective and label-free protein detection in physiological solutions using carbon nanotube transistors with nanobody receptors *Sensors Actuators* B **255** 1507–16
[168] Tung N T *et al* 2017 Peptide aptamer-modified single-walled carbon nanotube-based transistors for high-performance biosensors *Sci. Rep.* **7** 17881
[169] Tang X, Bansaruntip S, Nakayama N, Yenilmez E, Chang Y and Wang Q 2006 Carbon nanotube DNA sensor and sensing mechanism *Nano Lett.* **6** 1632–6
[170] Van Thu V, Tam P D and Dung P T 2013 Rapid and label-free detection of H5N1 virus using carbon nanotube network field effect transistor *Curr. Appl. Phys.* **13** 1311–5
[171] Feng W and Ji P 2011 Enzymes immobilized on carbon nanotubes *Biotechnol. Adv.* **29** 889–95
[172] Yang N, Chen X, Ren T, Zhang P and Yang D 2015 Carbon nanotube based biosensors *Sensors Actuators* B **207** 690–715
[173] Norouzi P, Larijani B, Ganjali M R and Faridbod F 2012 Admittometric electrochemical determination of atrazine by nano-composite immune-biosensor using FFT-square wave voltammetry *Int. J. Electrochem. Sci.* **7** 10414–26
[174] Gao N *et al* 2016 Specific detection of biomolecules in physiological solutions using graphene transistor biosensors *Proc. Natl Acad. Sci. USA* **113** 14633–8
[175] Gutiérrez-Sanz Ó, Andoy N M, Filipiak M S, Haustein N and Tarasov A 2017 Direct, label-free, and rapid transistor-based immunodetection in whole serum *ACS Sens.* **2** 1278–86
[176] Lee C W *et al* 2010 Solution-processable carbon nanotubes for semiconducting thin-film transistor devices *Adv. Mater.* **22** 1278–82
[177] Izard N *et al* 2008 Semiconductor-enriched single wall carbon nanotube networks applied to field effect transistors *Appl. Phys. Lett.* **92** 243112
[178] Sangwan V K *et al* 2011 Transfer printing approach to all-carbon nanoelectronics *Microelectron. Eng.* **88** 3150–4
[179] Deegan R D, Bakajin O, Dupont T F, Huber G, Nagel S R and Witten T A 1997 Capillary flow as the cause of ring stains from dried liquid drops *Nature* **389** 827–9
[180] Lazarescu M T 2013 Design of a WSN platform for long-term environmental monitoring for IoT applications *IEEE J. Emerg. Sel. Top. Circuits Syst.* **3** 45–54
[181] Someya T S, Small J, Kim P, Nuckolls C and Yardley J T 2003 Alcohol vapor sensors based on single-walled carbon nanotube field effect transistors *Nano Lett.* **3** 877–81
[182] Star A, Gabriel J-C P, Bradley K and Grüner G 2003 Electronic detection of specific protein binding using nanotube FET devices *Nano Lett.* **3** 459–63
[183] Bargaoui Y, Troudi M, Bondavalli P and Sghaier N 2018 Gate bias stress effect in single-walled carbon nanotubes field-effect-transistors *Diam. Relat. Mater.* **84** 62–5
[184] Lee S W *et al* 2012 Positive gate bias stress instability of carbon nanotube thin film transistors *Appl. Phys. Lett.* **101** 053504
[185] Won Lee S, Suh D, Young Lee S and Hee Lee Y 2014 Passivation effect on gate-bias stress instability of carbon nanotube thin film transistors *Appl. Phys. Lett.* **104** 163506
[186] Mattmann M *et al* 2010 Pulsed gate sweep strategies for hysteresis reduction in carbon nanotube transistors for low concentration NO_2 gas detection *Nanotechnology* **21** 185501
[187] Wang H, Cobb B, van Breemen A, Gelinck G and Bao Z 2014 Highly stable carbon nanotube top-gate transistors with tunable threshold voltage *Adv. Mater.* **26** 4588–93
[188] Helbling T, Hierold C, Roman C, Durrer L, Mattmann M and Bright V M 2009 Long term investigations of carbon nanotube transistors encapsulated by atomic-layer-deposited Al_2O_3 for sensor applications *Nanotechnology* **20** 434010
[189] Pop E 2008 The role of electrical and thermal contact resistance for Joule breakdown of single-wall carbon nanotubes *Nanotechnology* **19** 295202
[190] Collins P G, Arnold M S and Avouris P 2001 Engineering carbon nanotubes and nanotube circuits using electrical breakdown *Science* **292** 706–9
[191] Lee M, Noah M, Park J, Seong M-J, Kwon Y-K and Hong S 2009 'Textured' network devices: overcoming fundamental limitations of nanotube/nanowire network-based devices *Small* **5** 1642–8
[192] Wang Y, Pillai S K R and Chan-Park M B 2013 High-performance partially aligned semiconductive single-walled carbon nanotube transistors achieved with a parallel technique *Small* **9** 2960–9
[193] Lee M *et al* 2010 100 nm scale low-noise sensors based on aligned carbon nanotube networks: overcoming the fundamental limitation of network-based sensors *Nanotechnology* **21** 055504
[194] Okuda S, Okamoto S, Ohno Y, Maehashi K, Inoue K and Matsumoto K 2012 Horizontally aligned carbon nanotubes on a quartz substrate for chemical and biological sensing *J. Phys. Chem.* C **116** 19490–5
[195] Pugliese K M *et al* 2015 Processive incorporation of deoxynucleoside triphosphate analogs by single-molecule DNA polymerase I (Klenow Fragment) nanocircuits *J. Am. Chem. Soc.* **137** 9587–94
[196] Choi Y *et al* 2013 Dissecting single-molecule signal transduction in carbon nanotube circuits with protein engineering *Nano Lett.* **13** 625–31
[197] Sorgenfrei S *et al* 2011 Label-free single-molecule detection of DNA-hybridization kinetics with a carbon nanotube field-effect transistor *Nat. Nanotechnol.* **6** 126–32
[198] Wager J F 2014 Flat-panel-display backplanes: LTPS or IGZO for AMLCDs or AMOLED Displays? *Inf. Disp.* **30** 26–9
[199] Fukuda K and Someya T 2017 Recent progress in the development of printed thin-film transistors and circuits with high-resolution printing technology *Adv. Mater.* **29** 1602736
[200] Street R A 2009 Thin-film transistors *Adv. Mater.* **21** 2007–22
[201] Caraveo-Frescas J A, Nayak P K, Al-Jawhari H A, Granato D B, Schwingenschlögl U and Alshareef H N 2013 Record mobility in transparent p-type tin monoxide films and devices by phase engineering *ACS Nano* **7** 5160–7
[202] Rim Y S, Chen H, Liu Y, Bae S-H, Kim H J and Yang Y 2014 Direct light pattern integration of low-temperature solution-processed all-oxide flexible electronics *ACS Nano* **8** 9680–6
[203] Sheng J, Lee H-J, Oh S and Park J-S 2016 Flexible and high-performance amorphous indium zinc oxide thin-film transistor using low-temperature atomic layer deposition *ACS Appl. Mater. Interfaces* **8** 33821–8

[204] Jo J-W *et al* 2015 Highly stable and imperceptible electronics utilizing photoactivated heterogeneous sol-gel metal-oxide dielectrics and semiconductors *Adv. Mater.* **27** 1182–8
[205] Rembert T, Battaglia C, Anders A and Javey A 2015 Room temperature oxide deposition approach to fully transparent, all-oxide thin-film transistors *Adv. Mater.* **27** 6090–5
[206] Fukuda K, Takeda Y, Mizukami M, Kumaki D and Tokito S 2015 Fully solution-processed flexible organic thin film transistor arrays with high mobility and exceptional uniformity *Sci. Rep.* **4** 3947
[207] Pierre A, Sadeghi M, Payne M M, Facchetti A, Anthony J E and Arias A C 2014 All-printed flexible organic transistors enabled by surface tension-guided blade coating *Adv. Mater.* **26** 5722–7
[208] Hyun W J, Secor E B, Rojas G A, Hersam M C, Francis L F and Frisbie C D 2015 All-printed, foldable organic thin-film transistors on glassine paper *Adv. Mater.* **27** 7058–64
[209] Kim S H, Lee S H, Kim Y G and Jang J 2013 Ink-jet-printed organic thin-film transistors for low-voltage-driven CMOS Circuits with solution-processed AlO_X gate insulator *IEEE Electron Device Lett.* **34** 307–9
[210] Snell A J, Mackenzie K D, Spear W E, LeComber P G and Hughes A J 1981 Application of amorphous silicon field effect transistors in addressable liquid crystal display panels *Appl. Phys.* **24** 357–62
[211] Yang C-S, Smith L L, Arthur C B and Parsons G N 2000 Stability of low-temperature amorphous silicon thin film transistors formed on glass and transparent plastic substrates *J. Vac. Sci. Technol.* B **18** 683
[212] Powell M J, Glasse C, Green P W, French I D and Stemp I J 2000 An amorphous silicon thin-film transistor with fully self-aligned top gate structure *IEEE Electron Device Lett.* **21** 104–6
[213] Carey P G, Smith P M, Theiss S D and Wickboldt P 1999 Polysilicon thin film transistors fabricated on low temperature plastic substrates *J. Vac. Sci. Technol.* A **17** 1946–9
[214] Seok-Woon Lee and Joo S-K 1996 Low temperature poly-Si thin-film transistor fabrication by metal-induced lateral crystallization *IEEE Electron Device Lett.* **17** 160–2
[215] Wu M, Pangal K, Sturm J C and Wagner S 1999 High electron mobility polycrystalline silicon thin-film transistors on steel foil substrates *Appl. Phys. Lett.* **75** 2244–6
[216] Kelly A G *et al* 2017 All-printed thin-film transistors from networks of liquid-exfoliated nanosheets *Science* **356** 69–73
[217] Lin Z *et al* 2018 Solution-processable 2D semiconductors for high-performance large-area electronics *Nature* **562** 254–8